TECHNICAL REPORT 612

AN END EFFECT ASSOCIATED WITH CYLINDRICAL LANGMUIR PROBES ON THE EXPLORER XVII

BY

A. ANTHONY CHEN

N69-78538
(ACCESSION NUMBER) (PAGES) (NASA CR OR TMX OR AD NUMBER)
(THRU) (CODE) (CATEGORY)
FACILITY FORM 602

UNIVERSITY OF MARYLAND
DEPARTMENT OF PHYSICS AND ASTRONOMY
COLLEGE PARK, MARYLAND

AUGUST 1966

APPROVAL SHEET

Title of Thesis: An End Effect Associated with Cylindrical Langmuir Probes on the Explorer XVII

Name of Candidate: A. Anthony Chen
Master of Science, 1967

Thesis and Abstract Approved:

_____

Richard T. Bettinger
Assistant Professor of Physics
Department of Physics & Astronomy

Date Approved:

VITA

Name: Abraham Anthony Chen

Permanent Address: 6 Widcombe Road, Kingston 6, Jamaica

Degree and date to be conferred: Master of Science, 1967

Date of Birth: [redacted]

Place of Birth: [redacted]

Secondary Education: St. George's College, 1956

Collegiate Institutions Attended:	Dates	Degree	Date of Degree
Boston College, Chestnut Hill, Mass.	1957-1960	B.S.	1960
Harvard University, Cambridge, Mass.	1960-1961	M.A.T.	1961
University of Maryland, College Park, Md.	1963-1966	M.S.	1967

Major: Physics

Positions Held: Teacher, Catholic Memorial High School, Mass., 1961-1963.
Research Assistant, Physics Department, University of Maryland, 1964-1966.

ABSTRACT

Title of Thesis: An End Effect Associated with Cylindrical Langmuir Probes on the Explorer XVII

A. Anthony Chen, Master of Science, 1967

Thesis directed by: R. T. Bettinger, Assistant Professor of Physics

An anomaly has been observed in the ion current response of the cylindrical Langmuir probe carried aboard the Explorer XVII satellite. The anomaly consisted of a narrow peak with an amplitude greater than twice the normal response, when the axis of the probe was oriented parallel or nearly parallel to the velocity vector of the satellite. Bettinger (1966) has proposed that the source of the anomaly was the ion current entering through the end of the plasma sheath surrounding the probe and has derived an expression for this end effect current. Analysis of the Explorer XVII data in the present work showed good agreement with the end effect expression. The current given by this expression is proportional to $1/T_i^{3/4}$, were T_i = ion temperature. The end effect, therefore, has good prospects for ion temperature measurements.

AN END EFFECT ASSOCIATED WITH CYLINDRICAL LANGMUIR PROBES ON THE EXPLORER XVII

by

A. Anthony Chen

August 1966

Thesis submitted to the Faculty of the
Graduate School of the University
of Maryland in partial fulfillment of
the requirements for the degree of
Master of Science
1967

Acknowledgements

I wish to express my gratitude to all who have helped in this project; first of all, to Dr. R. T. Bettinger for his advice and encouragement and without whom this work would not have been possible; to J. Bohse for his valuable advise on computer programming; to J. Perez for computing and plotting the data in Fig. (14); to Dr. L. H. Brace and G. Dunham of Goddard Space Flight Center for providing the Explorer XVII data and other relevant information; and to Mrs. Donna Will for diligently typis this thesis.

This work has been supported by The National Aeronautics and Space Administration Grant NGR-21-002-060. A portion of the computer time for this project was supported by the facilities of the Computer Science Center of the University of Maryland.

TABLE OF CONTENTS

Chapter		Page
	INTRODUCTION	1
I.	THE IONOSPHERE	2
	A. Introduction	2
	B. UV Absorption	3
	C. Composition	4
	D. Temperature of Ionospheric Constituents	5
II.	LANGMUIR PROBE THEORY	8
	A. Plasma Sheath	8
	B. Normal Volt-Ampere Characteristics	8
	C. Anomalous Volt-Ampere Characteristics—An End Effect Theory	13
III.	THE LANGMUIR PROBE EXPERIMENT	20
	A. Description	20
	B. Ion Density Data	21
	C. Electron Temperature Data	22
IV.	DATA ANALYSIS	24
	A. Outline	24
	B. Aspect Determination	25
	C. Determination of Vehicle Potential	26
	D. Effective Probe Length	29
	E. Partial Densities of Ion Current with Two Constituents	33
	F. Data Correlation Program	35
	G. Results and Discussion	36

TABLE OF CONTENTS
(continued)

Chapter		Page
APPENDIX 1.	DETAILS OF ASPECT DETERMINATION	40
APPENDIX 2.	COMPUTER PROGRAMS	42
APPENDIX 3.	MAGNITUDE OF THE EFFECTIVE PROBE LENGTH CORRECTION	56
APPENDIX 4.	TANGENTIAL VELOCITY AT SHEATH EDGE	57
REFERENCES CITED		60
FIGURES		62

FIGURE CAPTIONS

Figure 1 COSPAR International Reference Atmosphere, 1964, showing the number density (logarithms to the base 10) vs. height for low solar activity and 14 hours local time.

Figure 2 COSPAR International Reference Atmosphere, 1964, showing the number density (logarithms to the base 10) vs. height for high solar activity and 14 hours local time.

Figure 3 Diagram illustrating the behavior of the altitude distribution of He^+, H^+, and O^+ in diffusive equilibrium assuming a given concentration at a reference level (which may lie above 500°km) and thermal equilibrium with T = 1200°K. This diagram was reproduced from Introduction to Space Science, edited by W. N. Hess, Gordon, and Breach Science Publishers, New York, 1965, with the permission of the editor.

Figure 4 Comparison of the volt-ampere characteristics given by equations (7) and (8) for various aspect angles and ion temperatures. (Equation (7) is temperature dependent.)

Figure 5 Plot of the total current collected vs. the voltage applied to the probe with the probe aspect listed at the top of the diagram.

Figure 6 The coordinate system fixed with respect to the probe. The arrows indicate the "drift" velocity of the particles relative to the probe.

Figure 7 End current vs. probe aspect with mass as parameter for a typical probe.

Figure 8 Location of instruments on the Explorer XVII satellite. The electron temperature probe and the ion density probe were interchangeable.

Figure 9 Functional diagram of the Langmuir probe.

Figure 10 Sample computer printout for the Explorer XVII ion density experiment.

Figure 11 Sample volt-ampere characteristics for the Explorer XVII electron temperature experiment.

Figure 12 Log-plot of the sample curve in Figure 11.

Figure 13 Diagram illustrating the probe aspect (C) and its projection (B) on the plane of rotation of the probe. A is the angle of closest approach of the probe to the vehicle velocity.

Figure 14 $R(= I/(dI/d\Psi))$ vs. Ψ . ($\Psi = eV/kT$)

Figure 15 Diagram illustrating the variation of the vehicle potential with probe aspect for a given pass.

Figure 16 Family of curves obtained by Walker (1965) with the potential ($\Psi = eV/kT$) as a function of sheath radius in Debye lengths. The curves were obtained by assuming an initial value of the radius (ρ_o) when $\Psi = -0.001$.

Figure 17 Curve a in Fig. (16) transformed from a log-plot to a linear plot.

Figure 18 Diagram illustrating the axial distance (d) that the particle must travel before being collected by the probe. A is the point where the particle enters the sheath.

Figure 19 Fit for BP595 with 10% H^+ and 90% O^+. The solid line represents the theoretical curve; the X's, the experimental curve with $\phi = K/r$; the dots, the experimental curve with $\phi = K/r^2$.

Figure 20 Fit for BP595 with 35% He^+ and 65% O^+. The solid line represents the theoretical curve; the X's, the experimental curve with $\phi = K/r$; the dots, the experimental curve with $\phi = K/r^2$.

Figure 21 Fit for COL831 with 17% H^+ and 83% O^+. The solid line represents the theoretical curve; the X's, the experimental curve with $\phi = K/r$; the dots, the experimental curve with $\phi = K/r^2$.

Figure 22 Diagram used to derive equations (35) and (36).

Figure 23 Magnitude of the effective probe length correction. Curve a represents the total current; curve b, the current given by equation (8) without correction; curve c, d, and e, the corrected currents using $\phi = K/r$, $\phi = K/r^2$, and $\phi = K/r^3$ respectively.

INTRODUCTION

On April 3, 1963 Explorer XVII, the first Aeronomy Satellite, was launched. The instruments carried aloft by the satellite included pressure gages for the measurements of the total neutral particle density, double focusing magnetic mass spectrometers for the measurements of the concentration of the neutral atmospheric constituents, and cylindrical Langmuir probes for the measurements of the electron temperature and ion density. The satellite itself was a 1 meter sphere with a perigee of 258 km and an apogee range of 920-870 km at middle Northern latitudes. It performed about 50 hours of useful work over a period of 100 days (SPENCER, 1965).

Data from the ion density experiment showed an anomalous peak in the current collected by the probes when the probe axis was oriented parallel or nearly parallel to direction of satellite motion (vehicle velocity). It will be shown that this phenomena can be explained in terms of the current collected through the ends of the plasma sheath surrounding the probe, and that analysis of the anomalous peak can become a useful method for determining ion temperatures in the ionosphere.

CHAPTER I

THE IONOSPHERE

Introduction

The ionosphere is an electrically neutral region containing a significant degree of ionization and displaying a relatively high electrical conductivity. The region extends from about 65 km to great distances and has been conventionally divided into the C, D, E and F regions according to the levels at which apparent peaks in the ionized particle concentration have been detected by ground based ionosondes. Rocket measurements have indicated that these layers are not necessarily characterized by a maximum concentration, but are often marked only by a "ledge" where the gradient is small. The C region lies at about 65 km with electron densities of the order of 10^2 cm^{-3}; the D region, between 70 and 85 km with electron densities of the order of 10^3 cm^{-3} at 80 km for an overhead sun; and the E region, between 85 and 150 km with noontime electron densities of the order of 10^5 cm^{-3} at 105 km. The region above 150 km is called the F region and is characterized by peaks ranging from 10^5 to 10^6 cm^{-3}. The lower F region, called the F_1 region, lies between 150 and 200 km with a broad peak, while the upper F region, called the F_2 region, exhibits a peak between 300 and 400 km.

UV Absorption

The properties of the ionosphere are largely controlled by the amount of solar uv radiation absorbed. Two processes are of importance, the photochemical process and photoionization. One of the more important photochemical reactions is the photodissociation of oxygen, which constitutes about 21% by volume of the atmosphere. The dissociation, $O_2 + h\nu \rightarrow O + O$ is caused by uv radiation of 2420 Å or less. The dominant reverse reaction is caused by a three body collision

$$O + O + M \rightarrow O_2 + M$$

where the third body, M, is usually necessary to conserve both momentum and energy. Since the concentration of M decreases and the radiation intensity increases with increasing altitude, atomic oxygen becomes dominant over molecular oxygen above 100 km. Only a small amount of dissociation of N_2, which constitutes about 78% by volume of the atmosphere, has been observed.

The photoionization process results in the formation of a positive ion and an electron. At low altitudes (<90km) the electrons have a high probability of undergoing collisional attachment to form negative ions. An important type of reaction for the loss of electron ion-pairs throughout the lower ionosphere is the dissociative recombination of positive molecular ions with electrons through the processes

$$N_2^+ + e \rightarrow N + N$$
$$O_2^+ + e \rightarrow O + O$$
$$NO^+ + e \rightarrow N + O$$

Loss can also occur by radiative recombination with an electron,

$$O^+ + e \rightarrow \bar{O} + h\nu$$

but the rate of recombination is slow.

Composition

Since direct measurements of the atmosphere are isolated in time and space, we refer to models for an overall picture of the atmospheric composition. Figures (1) and (2) show the COSPAR International Reference Atmosphere, 1964, for a neutral atmosphere based on all the satellite drag data available at that time. At low levels of solar activity, and 14 hours local time, the helium layer predominates at a lower altitude owing to the more rapid falloff of atomic oxygen. From the mass spectrometer experiment on the Explorer XVII satellite, which was designed to monitor $H_e(4)$, N(14), $H_2O(18)$, $O_2(32)$, $N_2(28)$ and O(16), Reber and Nicolet (1965) observed the average quiet daytime conditions near 260 km to be:

$$N_2,\ 1.5 \pm 0.5 \times 10^8\ cm^{-3};\ O,\ 2.4 \pm 0.4 \times 10^8\ cm^{-3};$$

$$H_e,\ 1.4 \pm 0.3 \times 10^6\ cm^{-3}.$$

These concentrations were somewhat less than those predicted by the model.

For the ionic constituents, mass spectrometer measurements showed that O_2^+ and NO^+ dominate below 200 km to 80 km (ISTOMIN and POKHUNDOV, 1963) and rf spectrometer measurements, that O^+ dominate from 200 km to at least 800 km (ISTOMIN, 1962). Other

data indicated a transition region from O^+ to H_e^+ between 800 km at 750°K and 1400 km at 1750°K, and a transition region from H_e^+ to H^+ at 3500 km and 1600°K (BOURDEAU and BAUER, 1963).

The region of the ionosphere above the F_2 peak is now considered as a teritiary ion mixture of O^+, H_e^+ and H^+ in diffusive equilibrium (AITKIN and BAUER, 1965). The distribution of an ion constituent, X_k^+, in diffusive equilibrium is

$$n(X_k^+) = n_o(X_k^+) \exp \left(-\int_o^z \left\{m(X_k^+) - [T_e/(T_i + T_e)]\, m_+\right\} (g/kT_i)dz\right) \quad (1)$$

where

$m(X^+)$ = ionic mass

m_+ = mean ionic mass

$= \Sigma\, n(X_i^+)\, m\,(X_i^+)\, /n\,(X_i^+)$

g = acceleration of gravity

T_i = ionic Temperature

T_e = electron Temperature

Fig. (3) shows the distribution of H_e^+, H^+ and O^+ assuming a given concentration, n_o, of these constituents at a reference level and $T_i = T_e = 1200°K$.

Temperature of Ionospheric Constituents

Hanson (1963) suggested that the electron temperature exceed the temperature of the ion and neutral particles, assumed to be in thermal contact, and the deviation is greatest in the lower F region. Only solar ultraviolet heating effects were considered. Below 200 km

photoelectrons injected into the atmosphere lose energy mainly by inelastic collisions. Above 200 km energy loss by elastic collisions with the ambient electrons is also important. Because the heat capacity of the electrons is several orders of magnitude smaller than the heat capacities of the other atmospheric constituents, the heat input from the photoelectrons will cause the ambient electron temperature to exceed the temperature of the other constituents. The difference in temperature depends on the processes which transfer heat from the relatively hot ambient electrons to the rest of the atmosphere, such as, coupling energy to the ions by coulomb collision and thermal coupling to molecular oxygen and nitrogen and atomic oxygen. Hanson also suggested that at high altitudes (above about 600 km) where the thermal contact between the ions and neutral particles begins to become small, the ion temperature begins to approach the electron temperature.

Dalgarno, McElroy and Moffet (1963) calculated that in a quiet ionosphere at noon the difference between the electron temperature and the temperature of the ions and neutral particles may reach a maximum value lying between 800°K and 1500°K near 200 km, and that the difference vanishes below 120 km and above about 400 km. Evans and Loewenthal (1964) have determined from incoherent backscatter observations that the ratio of electron temperature to ion temperature reached a maximum value ~2.2 at about 300 km soon after dawn. However, the conclusions were based on the assumption that the amount of H_e^+ at 300 km was negligible (<10%). If a small amount of H_e^+

was present, the results might have been interpreted as indicating an erroneously high value of T_i and low value of T_e/T_i. Spencer, Brace, Carignan, Taeusch and Niemann (1965) also determined that the electron temperature is greater than the molecular nitrogen temperature from measurements made between 140 and 300 km. The electron temperature experiment on the Explorer XVII satellite (BRACE, SPENCER, and DALGARNO, 1964) indicated a rapid rise in the average electron temperature from a nighttime value of about 1100°K to a mid-morning peak of 2700°K followed by an afternoon plateau of 2000°K. The corresponding neutral atmospheric temperature, calculated from density scale heights determined from measurements on the same satellite (NEWTON, HOROWITZ, PRIESTER, 1964), varied between a minimum near 500°K and a maximum of 1000°K.

CHAPTER II

LANGMUIR PROBE THEORY

Plasma Sheath

The Langmuir probe is an electrode or collector, usually of standard geometry, which is immersed in a plasma (in this case, the ionosphere) and whose volt-ampere characteristics may be interpreted in terms of the concentrations and energy distributions of the charged constituents of the plasma (ionosphere). When a conductor, such as the satellite-probe system, is immersed in a plasma, a charge sheath or contact potential region is formed between the plasma and the conductor. The sheath phenomena is due to the greater random speeds of the electrons, compared to those of the positive ions at thermal equilibrium, resulting in a great electron current to the conductor when it is intially immersed in the plasma. The conductor will, therefore, acquire a negative charge and its potential will be lowered until the flux of positive and negative charges equate. Thus a potential drop develops between the conductor and the plasma, the former being negative with respect to the latter. Therefore, for the satellite-probe system the satellite will have a negative potential with respect to the ionosphere and the net potential of the probe will be the sum of this vehicle potential and the applied voltage with which the probe is swept.

Normal Volt-Ampere Characteristics

The current collected by a stationary cylindrical probe immersed in a plasma has been discussed by Mott-Smith and Langmuir (1926). The sheath or contact potential region (surrounding the probe) was divided

into two parts, the central region toward which the positive ions were swept and where most of the potential drop was concentrated, and the outer region where the positive and negative charges were present in comparable quantities. Since the whole drop of potential in the outer region was small compared with the total, the sheath boundary was defined as the surface at which the sharp drop of potential began. It was also assumed that the ionized gas under consideration was of low density so that collisions within the sheath could be neglected, and it was further assumed that the composition of the charges was uniform about the collector and that their velocities were random, so that the sheath could be considered a circular cylinder of radius a concentric with the collector. Then if the density and velocity distributions were known at the sheath boundary, it was shown, by the simple mechanical principles of conservation of energy and angular momentum, that the current collected depended only on the initial velocities at the sheath edge and the potential drop across the sheath, independent of the potential distribution within the sheath. Several velocity distributions were considered, including the Maxwellian distribution, in which we are interested. The equations for current collection so derived were called the orbital motion equations. A similar discussion can be applied when the probe is driven positive with respect to the plasma.

For the case where the Maxwellian velocity distribution applies and where the sheath radius is much greater than the probe radius, the Mott-Smith-Langmuir equation for the particle current to a

cylindrical probe with an accelerating potential is

$$I = Ane(kT/2\Pi m)^{\frac{1}{2}} \ (2\Psi^{\frac{1}{2}}/\Pi^{\frac{1}{2}} + \exp(\Psi) \ \mathrm{erfc}(\Psi^{\frac{1}{2}})) \tag{2}$$

where

I = particle current

A = area of probe

n = ambient charge density

e = |charge of the particle|

k = the Boltzmann constant

T = particle temperature

m = mass of the particle

$\Psi = eV/kT$

V = |probe potential relative to the plasma|

$\mathrm{erfc}(\Psi^{\frac{1}{2}})$ is the complementary error function defined by

$$\mathrm{erfc}(z) = 2/(\Pi^{\frac{1}{2}}) \int_z^\infty e^{-t^2} \, dt = 1 - 2/(\Pi^{\frac{1}{2}}) \int_0^z e^{-t^2} dt$$

For $\Psi \geq 5$ equation (2) reduces to

$$I = Ane(kT/(2\Pi m))^{\frac{1}{2}} \ 2/(\Pi^{\frac{1}{2}}) \ (1 + eV/kT)^{\frac{1}{2}} \tag{3}$$

The slope of equation (3) reduces to

$$dI/dV = \frac{A}{2\Pi} \ ne^2(2/(eVm))^{\frac{1}{2}} \ (1/(1 + kT/eV))^{\frac{1}{2}} \tag{4}$$

For the "electron saturated" region where the probe is driven positive with respect to the plasma such that it attracts electrons, equation (4) is the primary means of determining the electron density, since m is known and $kT/eV \ll 1$. For the "ion saturated" region when the probe is driven negative and the thermal electrons are entirely

rejected, equation (4) gives the ion mass, if the ion (or electron) concentration is known.

The corresponding equation for the particle current to a probe with a retarding potential is

$$I = Ane(kT/(2\Pi m))^{\frac{1}{2}} \exp(-eV/kT) \tag{5}$$

Between the ion saturated region and the electron saturated region where the probe is negative but the electron current still dominates over the ion current, the electron temperature may be found by reducing equation (5) to the form

$$T = (e/K)\ (dV/d(\ln I)) \tag{6}$$

For experiments with satellite-borne probes where the probe velocity exceeds the thermal velocity of the ions for much of the flight, it is necessary to superimpose the drift velocity of the ions upon the Maxwellian distribution. Kanal (1964) obtained the following expression for the accelerated ion current collected by satellite-born probe, whose radius is much smaller than the sheath radius:

$$I_i = \left\{(kT_i/(2\Pi m_i))^{\frac{1}{2}}\ n_i\ e\ A\right\} \text{ times}$$

$$\left\{(2/\Pi^{\frac{1}{2}})e^{\Psi-x^2} \sum_{n=o}^{\infty} \frac{x^n}{n!\Psi^{n/2}} \text{ times}\right.$$

$$\left.\Gamma(n + 3/2,\Psi)\ J_n\ (2x\Psi^{\frac{1}{2}})\right\} \tag{7}$$

where the subscript i refers to the ions and

$x = u \sin \Theta/(2kT_i/m_i)^{\frac{1}{2}}$

u = vehicle velocity

Θ = angle between the velocity vector of vehicle and the axis of the probe (to be called probe aspect)

The expression $\Gamma(n + {}^3/2, \Psi)$ is the inverse of the incomplete gamma function

$$\Gamma(n + {}^3/2, \Psi) = \int_{\Psi}^{\infty} e^{-t}\, t^{n + \frac{1}{2}}\, dt,$$

and $J_n(2\chi\Psi^{\frac{1}{2}})$ is the n^{th} order Bessel function. Unfortunately the incomplete gamma function does not converge rapidly and equation (7) has limited use in data analysis.

By making use of the experimentally controllable condition, $kT_i << eV$, and by making a linear approximation for the Maxwellian velocity distribution, Bettinger (1965) obtained the following approximate expression for the accelerated ion current

$$I_i = 2r_p l n_i e (2/m_i)^{\frac{1}{2}} (eV + U)^{\frac{1}{2}} \qquad (8)$$

where:

$U = \frac{1}{2} m_i u^2 \sin^2\Theta$

r_p = probe radius

l = probe length

In Fig. (4) the values of the current given by equations (7) and (8) were plotted as functions as V. The values differed by less than 10% for the voltage range in which we were interested and for the range of temperature and probe aspects chosen. A computer program, LP13, to evaluate equation (7) is listed in Appendix 2. Unfortunately the range of the program is limited by overflow and underflow problems.

Anomalous Volt-Ampere Characteristics—An End Effect Theory

Fig. (4) and equation (8) indicate that the accelerated ion current should be a maximum when the probe axis is oriented at right angles to the velocity vector ($\Theta = 90$). Conversely the accelerated current should be a minimum when the probe aspect is 0^{o}. However the Explorer XVII Langmuir probe data showed that there was, in addition to the predicted maximum at 90^{o} orientation, a very strong peak centered around 0^{o} orientation. Fig. (5) gives the volt-ampere characteristics for two consecutive sweeps of one of the probes, and shows the peaks at 90^{o} and 0^{o} orientation. The source of the anomalous peak at 0^{o} appears to be the ion current flowing through the ends of the cylindrical sheath surrounding the probe, and which had been neglected in all previously mentioned calculations. Bettinger (1966) has derived an expression for this end-effect current and this thesis is intended to show the correlation between the anomalous current and the current predicted by the end-effect theory.

The following derivation of the end-effect current is due to Bettinger. We assume that the probe potential is negative and large enough so that the electron current can be neglected. Let $\bar{u}$ be the vehicle velocity and Θ the angle between the $\bar{u}$ vector and the axis of the probe (z axis). Let the space fixed coordinated system, in which there is no net plasma motion, be (r',ζ',z') where z' lies along the axis of the probe. Finally let the frame (r,ζ,z) be fixed with respect to the probe and moving with respect to the initial frame such that the velocity components are related by

$$\dot{r} = \dot{r}' + u \sin\Theta \cos\zeta \tag{9}$$

$$r\dot{\zeta} = r'\dot{\zeta}' + u \sin\Theta \sin\zeta \tag{10}$$

$$\dot{z} = \dot{z}' + u \cos\Theta \tag{11}$$

The situation is shown in Fig. (6). The arrows indicate the "drift" motion of the particles relative to the probe.

At the sheath edge the Maxwellian velocity distribution of one kind of particle with respect to the stationary coordinate system is

$$d^3N = n_i\left(\frac{m}{2\Pi kT}\right)^{3/2} \exp\left(-E/kT\right) r'\dot{r}'d\dot{\zeta}'d\dot{z}' \tag{12}$$

where the energy (E) is given by

$$E = \frac{m}{2}\left\{(\dot{r}')^2 + (r\dot{\zeta}')^2 + (\dot{z}')^2\right\} \tag{13}$$

For the moving system the new velocity distribution is

$$d^3N = n_i f(\dot{r},\dot{\zeta},\dot{z})\, r\, d\dot{r}\, d\dot{\zeta}\, d\dot{z} \tag{14}$$

where

$$f(\dot{r},\dot{\zeta},\dot{z}) = (\Pi^{1/2}v_o)^{-3}\exp\left\{-\frac{1}{v_o^2}\left[(\dot{r} - u \sin\Theta \cos\zeta)^2 + (r\dot{\zeta} - u \sin\Theta \sin\zeta)^2 + (\dot{z} - u \cos\Theta)^2\right]\right\} \tag{15}$$

and $v_o = \left(\frac{2kT}{m}\right)^{1/2}$, the most probable velocity of the particles. The current to the probe is then given by

$$i = e\int \dot{z}\, d^3N r dr d\zeta \tag{16}$$

where $rdrd\zeta$ is the element of area in the r-ζ plane.

The limits of integration depend mainly on angular momenta consideration. Since the $\dot{z}$ terms are unaffected, the limits are

$\pm \infty$. By applying the laws of conservation of energy and angular momentum to the charged particle trajectory in the sheath, we obtain the following condition for the collecting of a particle:

$$L^2/r_p^2 - L^2/r^2 \leq \dot{r}^2 + 2\Phi_p/m \tag{17}$$

where the unprimed variables refer to the particle on the z = o plane and the p subscript refers to the particle at the probe, and

$$L = \text{angular momentum per unit mass} = r^2\dot{\zeta} \tag{18}$$

Φ = electrostatic potential

The value of $\dot{r}^2$ is small compared to $2\Phi_p/m$ for the values of Θ in which we are interested. The limits of $\dot{r}$ are, therefore, also independent of the angular momenta criteria, and we can integrate between $\dot{r} = \pm \infty$. Rewriting equation (17) using equation (18) and setting $\dot{r} = 0$, we get

$$r^2\dot{\zeta}^2 \leq (2\Phi_p/m)\ (r_p^2/(r^2 - r_p^2)) \equiv \Sigma^2$$

making the limits of integration of $\dot{\zeta} = \pm \Sigma/r$

By equation (10) the upper limit on the thermal tangential velocity becomes

$$Y = \pm b - c \sin \zeta$$

where Y is the thermal component normalized in units of v_o and

$$b^2 = \frac{\Phi}{\frac{1}{2}mv_o^2} \quad \frac{r_p^2}{r^2 - r_p^2} \quad ,$$

$$c = (u/v_o) \sin \Theta$$

The limits on r and ζ are determined by the angular momenta criteria, and for a given value of ζ only particles up to a limiting radial distance, x, are collected. For the cold plasma case, the relation between x and ζ is obtained by setting Y = 0, and we get

$$x^2 = 1 + \Psi/(c^2 \sin^2 \zeta) \tag{19}$$

where

$x = r/r_p$, normalized radial component

$$\Psi = \Phi/(\tfrac{1}{2}mv_o^2) = \frac{eV}{kT}$$

When r = a = sheath radius and $x = x_a = a/r_p$, equation (19) becomes

$$\sin \zeta_o = b_a/c \qquad 0 \leq |\zeta_o| \leq \Pi/2 \tag{20}$$

where b_a is the value of b evaluated at r = a. For the thermal plasma case the relation between x and ζ is obtained by setting Y = 1, and we get

$$x^2 = 1 + \Psi/(1 + c \sin \zeta)^2 \tag{21}$$

When r = a, and $x = x_a$, we get two values of ζ:

$$\sin \zeta_2 = -(1 - b_a)/c \qquad 0 \leq |\zeta_2| \leq \Pi/2 \tag{22}$$

$$\sin \zeta_3 = -(1 + b_a)/c \qquad 0 \leq |\zeta_3| \leq \Pi/2 \tag{23}$$

Upon integrating over the allowed values of r and ζ and the other variables, we get the end current to be

$$i = 2n_i eu \cos\Theta \, r_p^2 \, I \tag{24}$$

where

$$I = \Pi/2 + \tfrac{1}{2}(x_a^2 - 1)\left\{(\zeta_2 - \zeta_3) - 2b_a(\zeta_2 + \zeta_3) - c(\cos\zeta_2 - \cos\zeta_3) - b_a^2 F(-\Pi/2,\zeta_3,c) - b_a^2 F(\zeta_2,\Pi/2,c)\right\} \tag{25}$$

$$F(\alpha,\beta,c) = \int_\alpha^\beta \frac{d\zeta}{1 + c\sin\zeta} \tag{26a}$$

$$= \frac{2}{(1 - c^2)^{\frac{1}{2}}} \arctan \frac{\tan\zeta/2 + c}{(1 - c)^{\frac{1}{2}}}\Bigg|_\alpha^\beta \qquad |c|<| \tag{26b}$$

$$= -c\tan(\Pi/4 - c\,\zeta/2)\Big|_\alpha^\beta \qquad |c|=1 \tag{26c}$$

$$= \frac{1}{(c^2-1)^{\frac{1}{2}}} \log\left\{\frac{\tan\zeta/2 + c - (c^2-1)^{\frac{1}{2}}}{\tan\zeta/2 + c + (c^2-1)^{\frac{1}{2}}}\right\}\Bigg|_\alpha^\beta \qquad |c|>1 \tag{26d}$$

For the Explorer XVII Langmuir probe experiment $b_a << 1$, so that $\zeta_2 \approx \zeta_3$ and equation (25) reduces to

$$I \approx \Pi/2 + \tfrac{1}{2}(x_a^2 - 1)\,(-2b_a(\zeta_2 + \zeta_3)) \tag{27a}$$

$$\approx \Pi/2 + \tfrac{1}{2}(x_a^2 - 1)\,4b_a \sin^{-1}(1/c) \tag{27b}$$

For the case where $a >> r_p$ equation (24) then becomes

$$i \approx 4n_i eu \cos\theta \; a \; r_p \left(\frac{eV}{kT}\right)^{1/2} \sin^{-1}(1/c) \tag{28}$$

The sheath radius, a, has been calculated by Bettinger and Walker (1965) to be

$$a = r_p + \frac{0.455\ (eV)^{3/4}}{n_i^{1/2}\, e(kT)^{1/4} \ln(a/r_p)} \tag{29}$$

Combining equations (28) and (29), we get

$$i \approx \frac{1.82 n_i^{1/2} \cos\theta\ r_p\ u\ (eV)^{5/4}}{\ln(a/r_p)\ (kT)^{3/4}} \sin^{-1}(1/c) \tag{30}$$

Equation (30) shows that an increasing thermal velocity will diminish the current by forcing more particles out of the sheath, and that the end current is related to the ion mass through the arc sine term,

$$i \propto \sin^{-1}(1/c)$$

$$= \sin^{-1}\left(\left(\frac{2kT}{m}\right)^{1/2} \frac{1}{u \sin\theta}\right)$$

Thus the lighter particles will have broader peaks centered around $\theta = 0^{\circ}$. Fig. (7) shows various peak profiles using ion mass as parameter. We also see that the current falls to one-half its maximum value when $c = (2)^{1/2}$. Thus the angular half width ($\theta^{1/2}$) is related to the ion temperature by the equation,

$$\sin \Theta_{\frac{1}{2}} = \frac{2}{u} \left(\frac{kT}{m} \right)^{\frac{1}{2}} \tag{31}$$

We will discuss these equations in more detail in Chapter IV.

CHAPTER III

THE LANGMUIR PROBE EXPERIMENT

Description

Two independent Langmuir probe systems, based on techniques developed in experiments with rockets, were used on the Explorer XVII Satellite to provide measurements of the ion density and the electron temperature of the ionosphere. Fig. (8) gives the locations of the instruments on the satellite and shows that the two Langmuir probes were almost diametrically opposite and situated on the equator of the satellite. Fig. (9) shows a functional block diagram of one of the probes. Each probe was 23 cm. in length and 0.056 cm. in diameter. A guard electrode, 10 cm. in length, was used to prevent the collection of charged particles within the sheath surrounding the satellite. The collector, guard and satellite skin were all made of stainless steel. For the ion density experiment the voltage applied between the probe and the satellite, Va, was a sawtooth sweep between -3.07v and +2.17v, with a sweep period of 2.03 sec. For the electron temperature experiment two sawtooth sweeps were employed (0 to +0.75v and 0 to +1.5v with a sweep period of 0.1 sec.) along with 2 linear current detectors of 1μa and 5μa full scale sensitivity which timed-shared the assigned telemetry channels on a 10-second-on, 10-second-off basis. The spin period of the satellite was about 0.7 seconds and the axis of spin was not necessarily perpendicular to the velocity vector of the satellite.

Ion Density Data

Fig. (5) gives a plot of the volt-ampere characteristics data points from the ion density probe for two consecutive sweeps, and shows the peaks at 90° and 0° orientations. The graph also shows a slight decrease in the value of the maximum current at 90°, $I_{max}\ (90^{\circ})$, between successive maxima corresponding to a change in applied voltage of about 1 volt. From curves such as that shown in Fig. (5) an emperical relationship between $I_{max}\ (90^{\circ})$ and the net voltage, V, was determined, showing that the value of $I_{max}\ (90^{\circ})$ at V = 0 was less than that of $I_{max}\ (90^{\circ})$ at data point voltages by 20% ± 3% (BRACE, SPENCER and DALGARNO, 1965). $I_{max}\ (90^{\circ})$ at V = 0 is simply the charge per unit time swept out by the frontal area of the collector. The ambient ion density is then given by equation (8), with V = 0 and $\Theta = 90$, as

$$n_i = (I_{max}\ (90^{\circ}))/(2rleu)$$

From the empirical relationship discussed above, the density is given by

$$n_i = (0.8\ I_{max}\ (90^{\circ}))/(2rleu) \qquad (32)$$

This method of determining the ion density is independent of the ion mass, a quantity not accurately known.

The data points used in Fig. (5) were taken from printouts from a computer program which Brace et al used to reduce the raw telemetry data to a readable form. Fig. (10) is a reproduction of a sample page of these printouts. The page contains data for 5

successive voltage sweeps of the probe. A few milliseconds after the onset of each sweep the current was recorded at intervals of 50 millisecs for 0.75 seconds. Thus, for each sweep there is a total of 15 current printouts, headed by the printout corresponding to near maximum negative voltage. The currents are given in units of 4.5×10^{-2} μa. Since the rate of change of voltage was known and the vehicle potential could be calculated, it was possible to find the net voltage corresponding to each printout within a few milliseconds. From the raw data Brace et al were also able to determine the probe aspects corresponding to the three highest current readings during each sweep. These aspects were listed below each sweep together with the time, in milliseconds, at which they were recorded. Unfortunately these values of the aspect are only fair (± a few degrees). Since the spin period of the satellite was known, it was possible to determine the probe aspect for the other current printouts by means of simple trigonometrical relations. Given at the bottom of each page are the ion densities calculated according to equation (32). Calibrations were done before the start of each set of 5 sweeps and are shown at the top of each page.

Electron Temperature Data

The electron temperature data were also reduced by computer. Fig. (11) is a reproduction of a sample volt-ampere curve plotted by computer. The current is given in units of 1.02×10^{-2} μa for the 5μa detector and $.147 \times 10^{-2}$ μa for the 1μa detector. Each unit on the abscissa is equivalent to 1.89×10^{-2} volts for the 5μa

detector and .94 X 10^{-2} volts for the 1μa detector. The probe aspect at the beginning and end of the curve is given at the top of the page. Fig. (12) shows a log-plot of the sample curve. The linear part of the plot represents the retarding potential region (Va + vehicle potential < 0) and the curved part represents the attracting potential region (Va + vehicle potential > 0). The electron temperature is determined from the linear part of the curve by the use of equation (6).

CHAPTER IV

DATA ANALYSIS

Outline

The process of isolating and analyzing the anomalous current involved the following steps: (1) The current printouts from the ion density experiment and the corresponding probe aspects, centered around 0^{o}, were determined; (2) All the normal currents which were expected to contribute significantly to the current printouts were subtracted from the values determined in step (1). The only significant current expected in this experiment was the accelerated ion current which entered through the sides of the sheath and was calculated by equation (8). Equation (8) had to be adjusted, firstly, to account for those particles which were forced out of the sheath by their axial velocities and were not collected, and secondly, to account for the fact that the ion current consisted of at least two constituents. Also, in order to find the net probe potential for use in equation (8), it was necessary to determine the vehicle potential; (3) The resulting anomalous current was normalized for density and voltage. For this purpose it was found that, for the parameters of the equation, the current could be related to the density and voltage according to the following equations

$$i/i_o = \left(V/V_o\right)^{1.2} \tag{33}$$

and

$$i/i_o = \left(n/n_o\right)^{0.55} \tag{34}$$

where the zero subscripts refer to the normalized values. Equations (33) and (34) agree closely with equation (30), which is an approximation. Finally the anomalous current was plotted as a function of the probe aspect and the graph compared to the theoretical curve obtained by equation (24) to show that the anomalous current can be explained by the end-effect theory.

Aspect Determination

Fig. (10) showed a sample page of the ion density data with the probe aspects corresponding to the three highest current printouts. Let C_1 and C_2 be two of these angles and B_1 and B_2, their corresponding projections on the plane of rotation of the probe. In Fig. (13) the plane of rotation is represented by three positions X, Y, Z of the probe. Z represents the position of closest approach to the direction of the vehicle velocity and A is the mimimum probe aspect. It can be shown (see appendix 1.) that

$$\cos A = \cos C_1/\cos B_1 = \cos C_2/\cos B_2 \tag{35}$$

and

$$B_2 = \arctan((\cos n\alpha - \cos C_1/\cos C_2)/\sin n\alpha) \tag{36}$$

where

α = angle the probe moves through in the XYZ plane in the interval between consecutive printouts (every 50 millisecs)

n = the number of intervals between C_1 and C_2

Equation (36) provided a means of calculating B_2 since the spin

period of the satellite, and therefore α, was a known quantity. Equation (35) then provided a means of calculating A. By subtracting α a suitable number of times from B_2, the projection, B_i, of a small probe aspect on the plane XYZ was found. The small probe aspect, C_i, was then obtained from equation (35),

$$C_i = \text{arc cos } (\cos A \cos B_i) \tag{37}$$

Program LP10 (see appendix 2) was used to calculate the desired values of C_i by the method described above. To identify which of the printouts corresponded to these values, the printouts of a given sweep were designated by the numbers 1 to 15 in the order in which they appeared from left to right, and LP10 was designed to give the location number of the printout that corresponded to a given C_i. Angles on one side of the peak at 0^o were arbitrarily designated negative.

Determination of Vehicle Potential

Equation (2) gives the accelerated electron current to the probe for the orbital-motion-limited mode as

$$I_e = An_e e \left\{kT_e/(2\pi m_e)\right\}^{\frac{1}{2}} \left\{2\psi^{\frac{1}{2}}/\pi^{\frac{1}{2}} + \exp(\psi)\ \text{erf}(\psi^{\frac{1}{2}})\right\} \tag{2a}$$

Then

$$dI_e/d\psi = An_e e\left\{kT_e/(2\pi m_e)\right\}^{\frac{1}{2}} \left\{\exp(\psi)\ \text{erf}(\psi^{\frac{1}{2}})\right\} \tag{38}$$

Letting

$$R = I_e/(dI_e/d\psi) \tag{39}$$

We get

$$R = 2\Psi^{\frac{1}{2}}/\left\{\Pi^{\frac{1}{2}}\exp(\Psi)\ \mathrm{erf}(\Psi^{\frac{1}{2}})\right\} + 1 \tag{39a}$$

Fig. (14) shows a plot of R as a function of Ψ. Referring to the electron temperature experiment, we see that, if T_e is determined from the retarding region of the curve, then R can be determined from the volt-ampere characteristics of the accelerating region by the use of equation (39). The value of Ψ corresponding to R for a given applied voltage, V_a, can be determined from Fig. (14). Therefore, the vehicle potential, V_v, can be found since

$$\Psi = eV_p/(kT_e)$$

$$V_p = V_a + V_v \tag{40}$$

where

V_p = probe potential relative to the plasma .

If V_v remains constant over a given range of applied voltages, then V_p can be found for any V_a over that range.

Because the size of the satellite was much greater than that of the probe it was expected that V_v would remain nearly constant during the applied voltage sweep and that V_p would increase by V_a according to equation (40). Table I shows a sample calculation of V_v for a given sweep by the method described above, and indicates that V_v became more negative as V_a increased. In such a case, equation (40) would still be satisfied but with V_p less positive than expected. A changing V_v for a given sweep was also indicated by the log plot (see Fig. (12)) which did not always show a clearly

TABLE I

CALCULATION OF VEHICLE POTENTIAL

$\Theta = -70^{\circ}$ at start of sweep
$\Theta = -123^{\circ}$ at end of sweep
$T_e = 2900^{\circ}K$
I_e in units of 1.02×10^{-2} μa
V_a, V_p, V_v in units of 1.9×10^{-2} volts

I_e	V_a	R	Ψ	V_p	V_v
99	35	1.50	.10	1	-34
124	40	1.68	.16	2	-38
152	45	1.86	.23	3	-42
184	51	2.38	.44	6	-45
211	56	2.76	.60	8	-48
237	61	3.25	.82	11	-50
269	67	3.58	.98	13	-54
298	72	3.69	1.03	14	-58
329	77	3.82	1.10	15	-62

Average vehicle potential = $-48 \times 1.9 \times 10^{-2}$ volts

= 0.9 volts

defined straight line for the retarding region, making the determination of T_e uncertain ($\pm$ 1000°K). Fortunately a value of $T_e \pm 1000^{\circ}K$ did not appreciably affect the value of V_V (less than 13%). Thus to determine the value of V_V for a single sweep a value of T_e was estimated and an average value of V_V determined from the calculations. It was also found that V_V varied with probe aspect and Fig. (15) shows a sample of the variation. It is possible to explain the variation in terms of a photo-electric effect. Since V_V did not remain constant over the range of applied voltages, the value of V_p could not be found accurately for any V_a, as was desired. Fortunately in the ion-density experiment with which we are concerned, the accelerated ion-current is not a strong function of V_p as can be seen from Fig. (4).

Effective Probe Length

Equation (8) had to be adjusted to account for those particles which were forced out of the sheath by their axial velocities and were not collected. The correction required a knowledge of the sheath thickness and the potential distribution within the sheath. Bettinger and Walker (1965) derived expressions for the sheath thickness, which in the case of a cylindrical probe is

$$(s^2 + 2ps)\ln(1 + s/p) = \Pi\Psi(1 + 2\Psi/3)^{\frac{1}{2}} \qquad (41)$$

where

s = sheath thickness in Debye lengths

Debye length (h) = $(kT/(4\Pi e^2 n))^{\frac{1}{2}}$

T = particle temperature

e = electronic charge

n = ambient charge density

p = probe radius in Debye lengths

Ψ = nondimensional potential = eV/kT

Equation (41) is functionally correct but the value of s determined had to be multiplied by a factor, ss, to fit the data.

The potential distribution within a cylindrical sheath about a small diameter probe is not well known. Walker (1965) has discussed the potential distribution within a spherical sheath, and we will assume that Walker's result is not greatly different from the cylindrical case. Fig. (16) shows a family of curves obtained by Walker with the potential represented as a function of sheath radius (ρ), given in Debye lengths. The curves were obtained by assuming an initial value, ρ_o, for the radius, where $\Psi = -0.001$ and calculating from ρ_o toward the origin. Curve a represents a typical curve in which we are interested ($\Psi \sim 30$, $p \sim .07$), and Fig. (17) shows curve a transformed from the log-plot to a linear plot. We can use this curve to determine the potential distribution within the sheath. Let the potential be represented by

$$\Phi = Kr^c \tag{42}$$

where

K and c are constants

r = radial distance from the probe axis = $(s + p)h$

then

$d\Phi/dr = c\ \Phi/r$

and

$$c = \left(r/\Phi\right)\left(d\Phi/dr\right) = \left(\rho/\psi\right)\left(d\psi/d\rho\right) \tag{43}$$

From Fig. (17) we obtained values of c ranging from -1.7 to -2.6. For the cylindrical probe we assumed that c = -1,-2,-3.

Knowing an approximate value for the sheath radius and the potential distribution, we can now calculate the length of the probe, d, that the particle must travel before being collected. Refer to the coordinate system fixed within the probe (see Fig. (6)). The particle energy E is given by

$$E = \tfrac{1}{2}m(\dot{r}^2 + r^2\dot{\zeta}^2 + \dot{z}^2) - \phi \tag{13}$$

Equations (13) and (18) combine to give

$$-dr/(2E/m - \dot{z}^2 - L^2/r^2 + 2\phi/m)^{\frac{1}{2}} = dt \tag{44}$$

Let t = 0, when r = a, the sheath thickness in cm. Then when $t = d/\dot{z}$, $r = r_p$, the probe radius. Integrating between the limits we get

$$d = -\dot{z}\int_a^{r_p} dr/(2E/m - \dot{z}^2 - L^2/r^2 + 2\phi/m)^{\frac{1}{2}} \tag{45}$$

This is the length of the probe that the particle must travel before being collected. It is obvious from Fig. (18) that the effective length of the probe is l-d. Any particle which enters the sheath below point A will be swept out of the sheath.

For $\phi = K/r$, the integration gives

$$- d/\dot{z} = (xr^2 + 2Kr/m - L^2)^{\frac{1}{2}} /x$$

$$- K/(mx^{3/2}) \ln\left\{K/m + xr + x^{\frac{1}{2}}(xr^2 + 2Kr/m - L^2)^{\frac{1}{2}}\right\} \Big|_a^{r_p} \qquad (46)$$

where

$$x = 2E/m - \dot{z}^2$$

For

$\phi = K/r^2$ we get

$$d = \dot{z}(\dot{r}_a a - \dot{r}_p r_p) /x \qquad (47)$$

where

$\dot{r}_a$ = radial velocity at $r = a$

$\dot{r}_p$ = radial velocity at $r = r_p$

$= (x - 2K/(ma^2) - L^2/r_p^2 + 2K/(mr_p^2))^{\frac{1}{2}}$

For $\phi = K/r^3$ Simpsons's $1/3$ rule was used to obtain the value of the integral. If n were the number of points to be used, and h the interal between each point then

$$h = (a - r_p) /n \qquad (48)$$

Since the error is approximately h^4, and we wanted d calculated to 2 significant figures, the value used for n was given by

$$(r_o - r_p)/n = (.01d/\dot{z})^{\frac{1}{4}} \qquad (49)$$

To calculate n by the above equation the value of d found for the k/r^2 case was used, since the k/r^2 and k/r^3 cases were not expected to differ by much. The magnitudes of the corrections using the three values for ϕ are discussed in Appendix 3.

The boundary conditions were all calculated in terms of $\dot{r}_a$, $a\dot{\zeta}_a$, (the tanential velocity at r = a), $\dot{z}$(the axial velocity, which was considered constant), a, r_p and K. $\dot{r}_a$ and $\dot{z}$ we calculated according to equations (9) and (11) in terms of their thermal velocities as

$$\dot{r}_a = \left(\frac{2kT_i}{3m}\right)^{\frac{1}{2}} + u \sin\Theta \cos\zeta_a \tag{50}$$

$$\dot{\zeta} = \left(\frac{2kT_i}{3m}\right)^{\frac{1}{2}} + u \cos\Theta \tag{51}$$

where

$\left(\frac{2kT_i}{3m}\right)^{\frac{1}{2}}$ is a component of the most probable thermal velocity.

$r_a\dot{\zeta}_a$ was determined from the following 3 equations, which are discussed in Appendix 4:

$$a\dot{\zeta}_a = 0.5(a\dot{\zeta}_a)_{max} \tag{52}$$

$$a\dot{\zeta}_a = \left(\frac{2kT_i}{3m}\right)^{\frac{1}{2}} - u \sin\Theta \sin\zeta_a \tag{53}$$

$$\left(a\dot{\zeta}_a\right)_{max} = \left(r_p/a\right)\left\{\frac{2kT_i}{3m} + 2\left(\frac{2kT_i}{3m}\right)^{\frac{1}{2}} u \sin\Theta \cos\zeta_a + 2\phi/m + u^2\sin^2\Theta\right\}^{\frac{1}{2}} \tag{54}$$

Partial Densities of Ion Current with Two Constituents

Use of equation (8) and the data from the ion density experiment indicated that the effective ion mass was less than 16(~10) at the altitudes under consideration (about 300 km - 450 km). It was

therefore assumed that the ion constituents at this altitude were 0^+, H^+, He^+. The total ion density determined in the experiment was, according to equation (32), independent of the type of ions being collected. However, in the use of equation (8) in the data analysis the mass of each constituent and its partial density had to be considered. A simple effective mass could not be used since the collected current depended upon the inverse square root of the mass. Instead the total current was obtained by calculating the partial densities and adding the currents corresponding to these densities. Unfortunately from the data available only 2 constituents could be considered at a time, 0^+ being the dominant constituent at all times.

Let n_o and n_H be the concentrations of 0^+ and H^+ respectively. Then equation (8) becomes

$$I_i = 2r_p e \left\{ l_H n_H (u^2 \sin^2\theta + 2eV/m_H)^{\frac{1}{2}} + l_o n_o (u^2 \sin^2\theta + 2eV/m_o)^{\frac{1}{2}} \right\} \tag{55}$$

where

m_H = mass of H^+

m_o = mass of 0^+

l_H = effective probe length for H^+

l_o = effective probe length for 0^+

$$n_o + n_H = n_i \tag{56}$$

and $l_H = l_o = 1$, when $\theta = 90^o$

By use of equation (55) and (56), n_o(and n_H) can be determined in terms of known quantities. Thus

$$n_o = \left. \frac{n_i(u^2 + 2eV/m_H)^{\frac{1}{2}} - I(90)/(2rle)}{(u^2 + 2eV/m_H)^{\frac{1}{2}} - (u^2 + 2eV/m_o)^{\frac{1}{2}}} \right|_{\Theta=90^o} \tag{57}$$

where

$I(90)$ = current printout at $\Theta \sim 90^o$

Since Θ is approximately 90^o, the end-effect current is negligible. Since the printouts for each voltage sweep of the ion density experiment contained current values corresponding to $\Theta \sim 90^o$ and a value of n_i, it was possible to determine n_o(and n_H) for each set of printouts. Then I_i can be determined from equation (55). A similar analysis applied for a O^+ and H_e^+ combination.

Data Correlation Program

Program LP20 (see Appendix 2) was the main computer program used in steps (2) and (3) outlined at the beginning of the chapter. The first part of the program rearranged the data in ascending order of probe aspect for easier plotting. Next the partial densities for each voltage sweep were calculated. Then for each printout d was calculated for both ion constituents with $\Theta = K/r$, K/r^2, and K/r^3 at an assumed ion temperature, and equation (55) was used to calculate the total ion current through the sides. The anomalous current, obtained by subtracting the above current from the total current, was then normalized for density and voltage for each printout and plotted as a function of probe aspect. The process could be

repeated for different temperatures. Subroutine VEHV was used to calculate the sheath thickness according to equation (41). Subroutine MAX was used to prevent data points from exceeding the limits set for the plotter. PLOTC, HXIS, SYMBOL, NUMBER and LINE were all University of Maryland subroutines from the Calcomp Plotter. Subroutine BRF was used to calculate the end-effect current given by equation (24) for 2 ionic constituents at different temperatures. LP20 is explained in detail in Appendix 2.

Results and Discussion

At zero probe aspect equation (28) reduces to

$$i \approx 2\Pi n_i e u a r_p \left(\frac{eV}{kT}\right)^{\frac{1}{2}}$$

Thus for a given sheath thickness the end current at $\Theta = 0^{\circ}$ does not depend upon the ion mass but upon the total ion density, so that the peak is a function, not of the type of ion combination, but of the temperature of the ion mixture, which is assumed to be in thermal equilibrium. This fact was taken into consideration in fitting the theoretical curves to the experimental data. The data from two passes were considered.

Pass No. 595 (BP595) occurred over Blossom Point, Maryland, on May 12 in sunlight with an altitude range of 272 to 292 km and a latitude range of 42 to 33 degrees and a speed of 7.9×10^5cm sec^{-1}. The average electron temperature and ion density were determined to be $2200^{\circ}K$ and 6.4×10^5 cm^{-3} respectively according to the methods described in Chapter III. The latter value was in close agreement with the value of the electron density which was

determined independently by the use of equation (4) and the electron curves similar to the one shown in Fig. (11). Equations (56) and (57) gave 10% H^+ and 90% O^+ for an oxygen-hydrogen combination. The value of ss was chosen to be 0.5. With values of ss = 0.6 and greater a correlation of peaks was achieved at the expense of too high a wing on the theoretical curve, while correlation in the region of the wings was achieved at the expense of too low a peak on the theoretical curve. With values of ss = .4 and smaller the best fit occurred at $T_i = 500^o$ K or less. Since the average neutral particle temperature ($\sim T_i$) determined from measurements made by the ionization guage sensors on the same satellite were greater then 500^o K in sunlight, we disregarded values of ss = 0.4 or less in favor of ss = 0.5. Fig. (19) shows the fit for $T_i = 750^o$K, ss = 0.5 and a ~ 1.4 cm. In the figure the X's represent points obtained by using $\phi = k/r$ and the dots, points obtained by using $\phi = k/r^2$. The points obtained by using $\phi = k/r^3$ are not included. However, they were only slightly higher than the corresponding points for $\phi = k/r^2$. It can be seen that the theoretical curve fits roughly between the corresponding X's and dots. The wing on the negative side of the experimental curve is lower than that on the positive side because of the presence of a small amount of electron current being collected (or conversely a small amount of ion current leaving). It can be seen from Fig. (10) that the currents corresponding to negative angles were collected at less negative probe potentials than the currents at positive angles. If the probe potential is small enough (V ~ -1.6 volts, $T_e \sim 3000^o$K),

the retarded electron current given by equation (5) is significant. An attempt was made to correct for the electron current, but the uncertainty in T_e provided enough scattering to nullify the effects of the correction and the latter was, therefore, omitted.

For the same pass equations (56) and (57) gave 35% H_e^+ and 65% O^+ for an oxygen-helium combination. Fig. (20) shows the fit for T_i = 750° K, ss = 0.5 and a ~ 1.4 cm. The high wing on the theoretical curve indicates that the H_e^+ concentration is too great. The most probable picture would be a combination of O^+, H^+ and H_e^+, with the H_e^+ concentration much smaller than 35%. Whatever the combination, the peak will still correspond to an ion temperature 750°K for ss = 0.5. The value of T_i chosen is in accordance with that which would be expected from the angular half width, which does not change appreciably over the range of temperatures used in obtaining the experimental curves. The half width is approximately 9.5° for the pass, and by equation (31) this corresponds to an ion temperature of about 830° K for an ion mass of 16.

Pass No. 831 (COL831) occurred in sunlight over College, Alaska, on May 28 with an altitude range of 440 to 363 km and a latitude range of 53 to 58 degrees and a speed of 7.8 X 10^5 cm sec^{-1}. The average electron temperature and ion density were determined to be 3700°K and 1.7 X 10^5 cm^{-3}. The latter value was lower than the value of 2.2 X 10^5 cm^{-3} for the electron density which was obtained by the use of equation (4) and the electron curves. The value of 2.2 X 10^5 cm^{-3} was used in the analysis since it gave more reasonable values for the oxygen-hydrogen composition. Equations (56) and (57)

gave 17% H^+ and 83% O^+ and the value of ss was chosen to be 0.5 to be consistent with the analysis of the previous pass. Fig. (21) shows the fit for T_i = 1250°K, ss = 0.5 and a ~ 2.2 cm. The high theoretical wing indicates that too great a value was used for the H^+ concentration. The wing on the negative side of the experimental peak is low for the same reason discussed in the analysis of the previous pass. Again the value of T_i (= 1250°K) chosen is in accordance with that calculated from the angular half width. For $\theta_{1/2}$ ~12.5° and an ion mass of 16, we get T_i ~1370° K. Equations (56) and (57) gave more H_e^+ than O^+ for an oxygen-helium combination. Since the hydrogen-oxygen combination resulted in already too high a value for H^+, we concluded that the H_e^+ concentration was negligible.

Analysis of COL831 and BP595 showed that the anomalous current can be explained in terms of the end-effect theory. With more data, better probe aspect and a knowledge of the ionic composition and potential distribution within the sheath, there will be better correlation between the experimental data and the theoretical curves and this method of analysis could become useful for ion temperature determination. Bettinger (1966) has discussed, in detail, the prospects of applying the end-effect results to determine ion temperature or vehicle velocity direction.

APPENDIX 1

DETAILS OF ASPECT DETERMINATION

The following is a derivation of equations (35) and (36): In Fig. (22) the arrow represents the direction of the vehicle velocity; Z is the position of the probe at closest approach to the vehicle velocity; Y is any other position of the probe; the side opposite angle A is a, and so on; the distance from the center of the satellite to the tip of the probe is 1.

Then

$$a^2 = 1^2 \tan^2 A$$

$$b^2 = 21^2 - 21^2 \cos B$$

$$c^2 = 1^2 + d^2 - 21d \cos C$$

But

$$d = 1/\cos A$$

Therefore

$$c^2 = 1^2 + 1^2/\cos^2 A - 21^2 \cos C/\cos A$$

By equating

$$c^2 = a^2 + b^2$$

We get upon reduction

$$\cos C \cos A = \cos B \cos^2 A$$

Thus

$$\cos A = \cos C/\cos B \qquad (35)$$

Referring to Fig. (13) and the notations on p.(25), we get

$$B_1 = B_2 + n\alpha$$

Therefore

$$\cos B_1 = \cos B_2 \cos n\alpha - \sin B_2 \sin n\alpha$$

Dividing by $\cos B_2$, we get

$$\cos B_1/\cos B_2 = \cos n\alpha - \tan B_2 \sin n\alpha$$

Therefore

$$\tan B_2 = (\cos n\alpha - \cos B_1/\cos B_2)/\sin n\alpha$$

But by equation (35)

$$\cos B_1/\cos B_2 = \cos C_1/\cos C_2$$

Thus

$$B_2 = \arctan \left[(\cos n\alpha - \cos C_1/\cos C_2)/\sin n\alpha\right] \qquad (36)$$

APPENDIX 2

COMPUTER PROGRAMS

Aspect Determination — LP10

Program LP10 was designed to tell by a simple counting procedure which of the printouts of a given sweep were centered around 0^{o} and to calculate the probe aspects corresponding to these printouts. The printouts were designated by the numbers 1 to 15 in the order in which they appeared on the printout sheets. C_1 and C_2 must have the same arbitrary sign (see Fig. 13) and $|C_1|>|C_2|$. The values assigned to QUANT and DIR can be best understood by referring to Fig. (10). If the low aspects occur to the right (left) of C_2, we make DIR a positive (negative) number. If, reading in the direction toward the low aspect and starting with C_1 or C_2 (whichever is farther away from the low aspects), we find that the initial magnitudes of the C's are decreasing (increasing), then we make QUANT a negative (positive) number. For instance, in the first set of printouts in Fig. (10) $C_1 = 107^{o}$, $C_2 = 81^{o}$, DIR = +2, QUANT = -1. The other variables are AINC, which is equal to the number of intervals between C_1, and C_2; POSI, the number designating the position of C_2; AMIN, the lowest probe aspect recorded for a given pass; and THETA, the number of radians the probe turns through between each printout.

Since C_1 and C_2 were not accurately determined, the use of equations (35) and (36) sometimes gave a value of COSA > 1. To correct for this a constant value of A was used for each pass. The value of A used was

the smaller of AMIN or an average value of those A's with cosine < 1. Then for each C_2 a new value of B_2 was found by use of equation (35). Next THETA was subtracted a suitable number of times from B_2 to give the values of B_i and equation (37) used to determine the C_i's. Program LP10 is listed on the following pages.

```
C      LP10
C      ASPECT AND VOLTAGE DETERMINATION
   10 FORMAT (F10.0)
   20 FORMAT (I5/(6F5.0))
   25 FORMAT(F10.5)
   30 FORMAT (F10.2, F10.0)
   40 FORMAT (1X///3X,5HANGLE,4X,7HVOLTAGE//1X)
   45 FORMAT(1X/1X,4HCOCA,2X,F10.5/1X)
   50 FORMAT (I5)
   60 FORMAT(1X///1X,4HAVGA,2X,F10.5,2X,2HAM,2X,F5.0///1X)
      DIMENSION C1(50),C2(50),QUANT(50),DIR(50),POS1(50),P(4),C3(50),
     1C4(50),C5(50),C6(50),VO3(50),VO4(50),VO5(50),VO6(50),AINC(50)
      READ (5,10) THETA
      READ (5,20) N,(C1(I),C2(I),QUANT(I),DIR(I),POS1(I),AINC(I),I=1,N)
      READ (5,25) AMIN
      NI = 4*N
      TOTA = 0.0
      AM = 0.0
      DO 75 I = 1,N
      SIGMA = THETA*AINC(I)
      C1BAR = .01745329*C1(I)
      C2BAR = .01745329*C2(I)
      PSI = (COS(SIGMA)-COS(C1BAR)/COS(C2BAR))/SIN(SIGMA)
      B = ATAN(PSI)
      IF (B) 52,54,54
   52 B2 = 3.1415927 + B
      GO TO 56
   54 B2 = B
   56 COCA = COS(C2BAR)/COS(B2)
      WRITE (6,45) COCA
      IF (COCA - 1.0) 70,70,75
   70 A = ATAN(SQRT(1./(COCA*COCA)-1.))
      TOTA = TOTA + A
      AM = AM + 1.0
   75 CONTINUE
      AVGA = TOTA/AM
      WRITE (6,60) AVGA,AM
      IF (AMIN-AVGA) 170,175,175
  170 COCA = COS(AMIN)
      GO TO 180
  175 COCA = COS(AVGA)
  180 DO 500 I = 1,N
      C2BAR = .01745329*C2(I)
      COCB2 = COS(C2BAR)/COCA
      B2 = ATAN(SQRT(1./(COCB2*COCB2)-1.))
      IF (COCB2) 76,77,77
   76 B2 = 3.1415927 - B2
      GO TO 79
   77 B2 = B2
   79 IF (QUANT(I)) 90,80,200
   80 QUATY = 0
   90 DO 100 JI = 1,10
      X = JI - 1
      BPRIME = B2 - X*THETA
      IF (BPRIME - THETA) 110,110,100
  100 CONTINUE
  110 XI = X
      GO TO 300
  200 Y = 0
  210 Y = Y + 1.
```

```
      BB = B2 + Y*THETA
      IF (3.1416 - BB) 220,220,210
  220 YI = Y
      BBPRI = 6.2832 - BB
      Z = 0
  230 Z = Z + 1.
      BPRIME = BBPRI - Z*THETA
      IF (BPRIME - THETA) 250,250,230
  250 ZI = Z
      XI = YI + ZI
  300 DO 350 J = 2,5
      AJ = J
      BA = BPRIME - (AJ -3.)*THETA
      COCC3 = COCA*COS(BA)
  350 P(J) = 57.29*ATAN(SQRT(1./(COCC3*COCC3)-1.))
      IF (DIR(I)) 370,360,380
  360 DCTN = 0.0
  370 C3(I) = -P(2)
      C4(I) = - P(3)
      C5(I) = P(4)
      C6(I) = P(5)
      POS2 = POS1(I) - XI
      V03(I) = POS2 + 1.
      V04(I) = POS2
      V05(I) = POS2 - 1.
      V06(I) = POS2 - 2.
      GO TO 500
  380 C3(I) = P(2)
      C4(I)=P(3)
      C5(I)=-P(4)
      C6(I)=-P(5)
      POS2=POS1(I) + XI
      V03(I)=POS2-1.
      V04(I)=POS2
      V05(I)=POS2+1.
      V06(I)=POS2+2.
  500 CONTINUE
      WRITE(6,40)
      DO 600 I=1,N
      WRITE (6,30) C3(I), V03(I)
      WRITE (6,30) C4(I),V04(I)
      WRITE (6,30) C5(I), V05(I)
  600 WRITE (6,30) C6(I),V06(I)
      WRITE(7,50) NI
      DO 700 I=1,N
      WRITE(7,30) C3(I),V03(I)
      WRITE(7,30)C4(I),V04(I)
      WRITE(7,30)C5(I),V05(I)
  700 WRITE (7,30) C6(I),V06(I)
      STOP
      END
```

Data Correlation - LP20

Program LP20 was used in steps (2) and (3) outlined in Chapter IV. ANGLE and VO1 are the probe aspects and their locations on the printouts page respectively. Cards for ANGLE and VO1 were punched by program LP10. Also

CURR1 = total current printout in units of 4.5 X 10^{-2} μa

DENI = total density

CURR2 = current printout at $\Theta \sim 90$

VO5 = voltage corresponding to CURR2

WEH = mass of H^+ or H_e^+ in amu

WEO = mass of O^+ in amu

RAD = probe radius

PSI = probe length

W = vehicle velocity

DE = standard density

VO4 = standard voltage

ADELT1 (ADELT2) = increment per inch on the vertical (horizontal) axis of the graph

TI = assumed ion temperature

LO = + 1 (-1) if the process is (is not) to be repeated using a new value of TI

Subroutine VEHV gave the voltage corresponding to the first printout of each sweep (VO3) as a function of the probe aspect. VO2 was the voltage corresponding to the printouts which were of

interest. Subroutine SHEATH calculated the sheath thickness (RO) in cm. SS was the factor used to multiply the sheath thickness calculated according to equation (41). Subroutine BRF calculated the end current according to equation (24). EL represented the partial densities and DENI, the total density. MI represented the ion masses and K, the difference between them. N was an integer used to repeat or stop the program. The main program and subroutines are listed on the following pages followed by a program (LP13) to calculate the current according to equation (7).

```
C     LP20
C     CALCULATION OF ANOMALOUS CURRENT
    5 FORMAT(1X/1X,23HLAST VALUES ENCOUNTERED/1X,2HWE,E10.3,2X,4HRDOT,
     1E11.4,2X,5HRCDOT,E11.4,2X,4HZDOT,E11.4,/1X,3HEL1,E10.3,2X,3HEL2,
     2E10.3,2X,3HEL3,E10.3,2X,2HRO,E10.3)
   10 FORMAT (I5/(F10.2,F10.0))
   20 FORMAT (I5/(F5.2,F8.0,F6.0,2F5.2))
   30 FORMAT(1X/2X,5HANGLE,2X,11HENDCURRENT1,2X,11HENDCURRENT2,
     12X,11HENDCURRENT3/1X)
   40 FORMAT( F7.2,2X,E11.4,2X,E11.4,2X,E11.4)
   50 FORMAT(4F5.0,2F10.0,3F5.0)
   60 FORMAT(1X////1X,2HSS,2X,E10.4/1X,
     1          2HDE,2X,E10.4/1X,1HW,2X,E10.4/1X,2HMH,2X,E10.4/1X,
     22HTI,2X,E10.4/1X, 3HVO4,2X,E11.4/1X,2HMO,2X,E10.4)
   70 FORMAT(F5.0,I2,F3.0)
      DIMENSIONVO5(200),ANGLE(200),VO1(200),CURR1(200),Y(1001),
     1CURR2(200),DENI(200),          CEND1(200),          D(1000),
     2CEND2(200),CEND3(200),DENO(200),DEH(200),VOLT(200),
      READ (5,10) N,(ANGLE(I),VO1(I),I = 1,N)
      READ(5,20)N,(CURR1(I),DENI(I),        CURR2(I),VO5(I),I=1,N)
      READ(5,50)WEH,WEO,RAD,PSI,W,DE,VO4,ADELT1,ADELT2
C     DATA IN ASCENDING ORDER
      NI=N-1
      DO 82  I=1,NI
      IPI=I+1
      DO 82  J=IPI,N
      IF(ANGLE(I)-ANGLE(J)) 82,82,86
   86 ALPHA= ANGLE(I)
      ANGLE(I)=ANGLE(J)
      ANGLE(J)=ALPHA
      ALPHA=VO1(I)
      VO1(I)=VO1(J)
      VO1(J)=ALPHA
      ALPHA=CURR1(I)
      CURR1(I)=CURR1(J)
      CURR1(J)=ALPHA
      ALPHA=DENI(I)
      DENI(I)=DENI(J)
      DENI(J)=ALPHA
      ALPHA=TEMP(I)
      TEMP(I)=TEMP(J)
      TEMP(J)=ALPHA
      ALPHA=CURR2(I)
      CURR2(I)=CURR2(J)
      CURR2(J)=ALPHA
      ALPHA=VO5(I)
      VO5(I)=VO5(J)
      VO5(J)=ALPHA
   82 CONTINUE
      CALL PLOTS(D,1000)
      MH=WEH
      MO=WEO
      K=MO-MH
      GAMMAH=1.915E12/WEH
      GAMMAO=1.915E12/WEO
      DEO=0.0
      FACT1=3.204E-13*RAD*PSI
      DO 100 I=1,N
      CALL VEHV(ANGLE(I),VO3)
      VO2=VO3-(VO1(I)-1.0)*0.146
```

```
      FACT2=SQRT(W**2+GAMMAH*VO5(I))
      FACT3=SQRT(W**2+GAMMAO*VO5(I))
      CURR7=CURR2(I)*4.5E-2
C     CALC PARTIAL DENSITIES
      DENO(I)=(DENI(I)*FACT2-CURR7   /FACT1)/(FACT2-FACT3)/DENI(I)
      DEH(I)=1.0-DENO(I)
      DEO=DEO+DENO(I)
  100 VOLT(I)=VO2
   80 READ(5,70) TI,LO,SS
      WRITE(6,60) SS,DE,W,WEH,TI,VO4,WEO
      DO 200 I = 1,N
      VO2=VOLT(I)
      DENH=DEH(I)
      THETA = .01745329*ABS(ANGLE(I))
      USIN= W*SIN(THETA)
      SIGMA= USIN**2
      CALL SHEATH (TI,DE,VO2,RAD,SS,RO)
      TERM1= 0.0
      TERM2= 0.0
      TERM3= 0.0
      RATIO= RAD/RO
      WE= WEH
  110 TV1= .550E8*TI/WE
      TV2= SQRT(TV1)
      GAMMA= 1.915E12/WE
      PS = GAMMA*VO2
      TV3= TV1+ PS + SIGMA
C     CALC EFFECTIVE PROBE LENGTH
      DO 300 IA= 1,90
      AI=IA
      RHO= .01745329*AI
      TV3A= TV3+ 2.*TV2*USIN*COS(RHO)
      RHS= TV2- .5*RATIO*SQRT(TV3A)
      OS= USIN*SIN(RHO)
      IF (RHS- OS) 310,310,300
  300 CONTINUE
  310 COCAVG= COS(RHO)
      RCDOT= RATIO*SQRT(TV3+ 2.*TV2*USIN*COCAVG)*.5
      RDOT= TV2+ USIN*COCAVG
      ZDOT= TV2+ W*COS(THETA)
      R= RAD
      EM= RCDOT**2+ RDOT**2
      CONST1= PS /2.*RAD
      ANMO2= (RO*RCDOT)**2
      SUM1= 0.0
  320 R2= SQRT(ABS(EM*R**2+ 2.*CONST1*R- ANMO2))
      R3= ALOG(CONST1+ EM*R+ EM**0.5*R2)
      SUM1= R2/EM- CONST1*R3/EM**1.5- SUM1
      IF(R-RAD) 340,330,340
  330 R= RO
      GO TO 320
  340 EL1= ZDOT*SUM1
      IF (PSI-EL1)115,115,120
  115 EL1= PSI
  120 PSI1= (PSI- EL1)/PSI
      CONST2= CONST1*RAD
      RPDOT= SQRT(ABS(EM+(2.*CONST2- ANMO2)/RAD**2-2.*CONST2/RO**2))
      EL2= ZDOT*(RDOT*RO- RPDOT*RAD)/EM
```

```
      IF(PSI -EL2) 130,130,140
  130 EL2= PSI
  140 PSI2= (PSI- EL2)/PSI
      CONST3= CONST2*RAD
      N1= (RO-RAD)/(ABS(.01*EL2/ZDOT))**0.25
      N2=(N1/2)*2
      IF(1000- N2) 142,142,145
  142 N2= 1000
  145 FN= N2
      H= (RO-RAD)/FN
      N3= N2+ 1
      DO 150 IB=1,N3
      BI= IB-1
      R= RAD+ H*BI
  150 Y(IB)= 1./SQRT(ABS(EM+ 2.*CONST3/R**3-ANMO2/R**2))
      SUM= 0.0
      KI= N2/2- 1
      DO 160 J=1,KI
  160 SUM= SUM+ 4.*Y(2*KI)+ 2.*Y(2*KI+1)
      EL3= ZDOT*(H/3.*(Y(1)+ SUM+4.*Y(N2)+ Y(N3)))
      IF (PSI- EL3) 170,170,180
  170 EL3= PSI
  180 PSI3= (PSI- EL3)/PSI
      FACTH= DENH*SQRT(SIGMA+ GAMMA*VO2)
      TERM1= TERM1+ FACTH*PSI1
      TERM2= TERM2+ FACTH*PSI2
      TERM3= TERM3+ FACTH*PSI3
      IF( WE- WEH) 370,360,370
  360 DENH= DENO(I)
      WE= WEO
      GO TO 110
  370 DENSY= DENI(I)
      CTOT= CURR1(I)*4.5E-2
      TERM4= FACT1*DENSY
      CENDA= ABS(CTOT- TERM4*TERM1)
      CENDB= ABS(CTOT- TERM4*TERM2)
      CENDC= ABS(CTOT- TERM4*TERM3)
      TERM5= (DE/DENSY)**.55*(VO4/VO2)**1.2
      CEND1(I)= CENDA*TERM5
      CEND2(I)= CENDB*TERM5
      CEND3(I)= CENDC*TERM5
  200 CONTINUE
      WRITE(6,5) WE,RDOT,RCDOT,ZDOT,EL1,EL2,EL3,RO
      WRITE (6,30)
      WRITE (6,40) (ANGLE(I),CEND1(I),CEND2(I),CEND3(I), I=1,N)
      CALL MAX(CEND1,N)
      CALL MAX(CEND2,N)
      CALL MAX(CEND3,N)
      CALL PLOTC(( .0,-11.0,-3)
      CALL PLOTC(12.0,0.5,-3)
      CALL AXIS(5.0,0.0,7HCURRENT,7,10.0,90.0,0.0,ADELT1)
      CALL AXIS ( 0.0,0.0,6HASPECT,-6,10.0,0.0,-50.0,ADELT2)
      CALL SYMBOL(0.0,9.0,0.2,2HTI,0.0,2)
      CALL NUMBER(0.6,9.0,0.2,TI,0.0,-0)
      CALL SYMBOL(0.0,8.4,0.2,2HRO,0.0,2)
      CALL NUMBER(0.6,8.4,0.2,RO,0.0,2)
      CEND1(N+1)=0.0
      CEND1(N+2)=ADELT1
```

```
      ANGLE(N+1)=-50.0
      ANGLE(N+2)=ADELT2
      CALL LINE(ANGLE,CEND1,N,1,-1,4)
      CEND2(N+1)=0.0
      CEND2(N+2)=ADELT1
      CALL LINE(ANGLE,CEND2,N,1,-1,9)
      CEND3(N+1)=0.0
      CEND3(N+2)=ADELT1
      CALL LINE(ANGLE,CEND3,N,1,-1,8)
      IF(LO) 210,80,80
  210 CALL PLOTC(18.0,0.0,-3)
      CALL PLOTC(0,0,999)
      AN=N
      DEOAVG =DEO/AN*DE
      CALL BRF(VO4,RAD,DEOAVG,W,DE,K,MO)
      STOP
      END



      SUBROUTINE \EHV(ASPECT,VO3)
C     COL831 VEHICLE POTENTIAL
      IF (ASPECT+25.0)20,20,30
   20 VO3=3.98-0.48E-2*ASPECT
      RETURN
   30 IF(ASPECT+12.0)40,40,50
   40 VO3=3.72-1.53E-2*ASPECT
      RETURN
   50 IF(ASPECT-42.0)60,60,70
   60 VO3=3.90
      RETURN
   70 VO3=4.41-1.21E-2*ASPECT
      RETURN
      END


      SUBROUTINE SHEATH (TI,EL,VP,RP,SS,RO)
      A1=6.9*SQRT (ABS (TI/EL))
      PSI=0.1161E05*VP/TI
      A2=      PSI*SQRT (ABS (1.+(2.*PSI/3.)))*3.1416
      S=SQRT (ABS (A2))
   12 A3=2.*RP*S/A1
      A4=ALOG(ABS (1.+(S*A1/RP)))
      A5=((S*S)+A3)*A4
      IF (ABS (A2-A5)-(.01*A2)) 16,16,14
   14 S=SQRT (ABS ((A2/A4)-A3))
      GO TO 12
   16 RO= S*A1*SS
      RETURN
      END


      SUBROUTINE MAX(CURR,N)
C      MAX CTOT FOR COL831
      DIMENSION CURR(200)
      DO 100 K=1,N
      IF(CURR(K)- 0.1) 100,100,50
```

```
   50 CURR(K)= 0.1
  100 CONTINUE
      RETURN
      END


      SUBROUTINE BRF(VP,RP,EL,VS,DENI,K,MI)
C     CALC OF END CURRENT BY EQUATION(24)
    1 FORMAT(1E12.6,   I3)
    2 FORMAT (1X//2X,2HVP,2X,E10.4/2X,2HRP,2X,E10.4/3X,1HN,2X,E10.4/2X,
     1 2HMI,2X,I2/2X,2HTI,2X,E10.4/2X,2HVS,2X,E10.4/2X,2HSS,2X,E10.4
     2 ///////4X,5HTHETA,8X,1HC,11X,7HCURRENT)
    4 FORMAT(10E12.4)
      DIMENSION FOT(200)
      PI=1.5708
    5 READ(5,1)SS,   N
   10 DO100 J=1,15
      QUEST=-1.0
C     VALUE OF ION TEMPERATURE
  110 TI=250*(J-1)
C     SHEATH CALCULATION
      A1=6.9*SQRT (ABS (TI/DENI))
      PSI=0.1161E05*VP/TI
      A2=2.*PI*PSI*SQRT (ABS (1.+(2.*PSI/3.)))
      S=SQRT (ABS (A2))
   12 A3=2.*RP*S/A1
      A4=ALOG(ABS (1.+(S*A1/RP)))
      A5=((S*S)+A3)*A4
      IF (ABS (A2-A5)-(.01*A2)) 16,16,14
   14 S=SQRT (ABS ((A2/A4)-A3))
      GO TO 12
   16 S=SS*S
      WRITE(6,2)VP,RP,EL,MI,TI,VS,SS
      A=(S*A1)+RP
      XA=(A*A/(RP*RP))-1.
      BA=SQRT (ABS (PSI/XA))
C     VALUE OF ASPECT
      NI=1
      NTI=0
   17 NTI=NTI+NI
      IF(NTI-182) 18,18,120
  120 IF(QUEST)220,220,130
  130 EL=DENI-EL
      MI=MI+K
      GO TO 100
   18 IF (NTI-20) 23,23,19
   19 NI=2
      IF (NTI-40) 23,23,21
   21 NI=10
   23 ETD=NTI
      ETD=(ETD-1.)/2.
      BMI=MI
      VO=.1287E05*SQRT (ABS (TI/BMI))
      SET=ETD*PI/90.
      C=VS*SIN (SET)/VO
      C1=SQRT (ABS (1.-(C*C)))
C     CALC OF EQN(24)
      IF (C)  20,20,13
```

```
 13 SEO=(.1E07/(VS*SIN (SFT)))*SQRT (ABS ((1.915*VP)/(XA*BMI)))
    IF (1.-SEO) 20,20,22
 20 SEO=1.
    CEO=0.
    EO=PI
    GO TO 25
 22 CEO=SQRT (ABS (1.-(SEO*SEO)))
    EO=ATAN (SEO/CEO)
 25 IF (C) 24,24,11
 11 SE2=(1.-BA)/C
    IF (1.-ABS (SE2)) 24,24,26
 24 SE2=(1.-BA)/ABS (1.-BA)
    CE2=0.
    E2=PI
    TE22=.1E+30*SE2
    GO TO 29
 26 CE2=SQRT (ABS (1.-(SE2*SE2)))
    E2=ATAN (SE2/CE2)
    TE22=SIN (E2/2.)/COS (E2/2.)
 29 IF (C) 28,28,27
 27 SE3=(1.+BA)/C
    IF (1.-SE3) 28,28,30
 28 SE3=1.
    CE3=0.
    E3=PI
    TE32=.1E+30
    GO TO 33
 30 CE3=SQRT (ABS (1.-(SE3*SE3)))
    E3=ATAN (SE3/CE3)
    TE32=SIN (E3/2.)/COS (E3/2.)
 33 IF (C-1.) 34,36,38
 34 F2=0.-(2.*BA*BA/C1)*(ATAN ((1.+C)/C1)+ATAN ((TE22-C)/C1))
    GO TO 40
 36 F2=0.-(BA*BA)*SIN ((PI+E2)/2.)/COS ((PI+E2)/2.)
    GO TO 40
 38 F2A=ALOG(ABS ((C-C1-TE32)*(C+C1-1.)/((C+C1-TE32)*(C-C1-1.))))
    F2B=ALOG(ABS ((1.+C-C1)*(C+C1-TE22)/((1.+C+C1)*(C-C1-TE22))))
    F2= -BA*BA*(F2A+ F2B)/C1
 40 FM= F2+ E3- E2+ 2.*BA*(E2+E3)+ C*(CE3- CE2)
    FO=0.16E-18*EL*VS*RP*RP*(2.*PI+XA*FM)*COS(SET)
    IF (QUEST) 200,200,300
200 WRITE (6,4) ETD,C,FO,EO,E2,E3,BA,CE3,CE2,F2
    KXX=2.0*(ETD+0.5)
    FOT(KXX)=FO
    GO TO 17
220 EL=DENI-EL
    MI =MI-K
    QUEST=2
    GO TO 110
300 KXX=2.0*(ETD+0.5)
    FO=FOT(KXX)+FO
    WRITE (6,4) ETD,C,FO,EO,E2,E3,BA,CE3,CE2,F2
    GO TO 17
100 CONTINUE
    IF (N) 5,5,44
 44 RETURN
    END
```

```
C     CALC KANAL FORMULA  LP13
      DOUBLE PRECISION VO, TE, TEMP1, SUM1, SUMK, TOT, AK, AKINC, TOT1,
     1TOTK, FK, FKINC, DN, TERM3, EI, PRON, TERM2, TEMP6, TERM5, AM,
     2AKSUM,ROOT1
   10 FORMAT(D15.4,3F10.0,3F5.0,I5)
   15 FORMAT (1X,2HTH,3X,E13.6/1X,2HTE,3X,D13.6/1X,1HW,4X,E13.6/1X,2HDE,
     13X,E13.6/1X,2HWE,3X,E13.6)
   17 FORMAT(1X/4X,1HN,10X,5HKTERM,4X,1HK,10X, 5HJTERM,4X,1HJ,11X,
     14HTERM/1X)
   20 FORMAT(1X////1X,7HVOLTAGE,3X,E10.4,5X,7HCURRENT,3X,E13.5,
     12X,6HTERMNO,E13.5////1X)
   35 FORMAT(1X/1X,3HTOT,2X,D25.16,2X,1HK,I5,2X,4HSUM2,2X,E13.6,2X,1HJ,
     1I5)
   50 FORMAT(I5,2X,D13.6,I5,2X,E13.6,I5,2X,E13.6)
  110 FORMAT (1X//1X,8HOVERFLOW)
  150 READ(5,10) TE,THETA,W,DE,WE,RAD,PSI,LO
      CID = 3.64816E-9*DE*RAD*PSI*SQRT(TE/WE)
      TEMP2 = 1.285E04*SQRT(TE/WE)
      WRITE (6,15) THETA,TE,W,DE,WE
      TEMP3 = W*SIN(THETA)/TEMP2
      DO 500 M=1,15
      WRITE (6,17)
      AM = M
      VO = 3.0D0 - AM*0.2D0
      TEMP1 = 1.160555302583252D04*VO/TE
      ROOT1 = DSQRT(TEMP1)
      TEMP5 = TEMP1 - TEMP3**2
      TEMP4 = 1.1284*EXP(TEMP5)
C     INITIALIZE, N=0
      SUM1=2.0D0/3.0D0
      SUMK = 2.0D0/3.0D0
      AKSUM= 1.0E37
      TEMPA= TEMP1*ROOT1
      DO 190 K= 1,400
      AK = K
      SUMK = (-1.0D0)*SUMK*TEMP1*(AK +0.5D0)/(AK*(1.5D0+AK))
  180 SUM1 = SUM1 + SUMK
      TOT = .8862269254527580- SUM1*TEMPA
      IF( ABS(AKSUM- TOT )- .01*AKSUM) 210,190,190
  190 AKSUM= TOT
  210 SUM2 = 1.
      SUMJ = 1.
      SUM2A= 1.0E37
      DO 255 J= 1,300
      AJ = J
      SUMJ=(-1.)*SUMJ*TEMP3**2*TEMP1/(AJ*AJ)
  250 SUM2 = SUM2 + SUMJ
      IF(ABS(SUM2A- SUM2)- .01*SUM2A) 260,255,255
  255 SUM2A= SUM2
  260 TERMNO = TOT*SUM2
      N=0
      WRITE (6,50) N,TOT,K,SUM2,J,TERMNO
C     INITIALIZED, N=0
      TERM2 = .8862269254527580
      TERM1 = 1.0
      REFACN = 1.0
      DO 400 N=1,100
      DN = N
      TERM1=TERM1*TEMP3/(DN*ROOT1)
      TERM2 = TERM2*(2.0D0*DN+1.0D0)/2.0D0
```

```
C       INITIALIZE, K = 0
        TEMP6=TEMP1**(N+1)*ROOT1
        IF(1.0D38-TEMP6)440,440,280
  280   TOT1 = 1.0D0/(DN+1.5D0)
        TOTK = 1.0D0/(DN+1.5D0)
        AKTOT= 1.0E37
        DO 285 K= 1,400
        FK = K
        TOTK=(-1.0D0)*TOTK*TEMP1*(DN+FK+0.5D0)/(FK*(DN+1.5D0+FK))
  282   TOT1 = TOT1 + TOTK
  295   TERM3 = TOT1*TEMP6
        TERM5 = TERM2 - TERM3
        IF( ABS(AKTOT-TERM5)- .01*AKTOT) 290,285,285
  285   AKTOT= TERM5
C       INITIALIZE J =0
  290   REFACN=REFACN/DN
        TOTJ=REFACN
        TOT2=REFACN
        AJTOT= 1.0E37
        DO 325 J= 1,300
        BJ = J
        TOTJ = (-1.)*TOTJ*TEMP3**2*TEMP1/(BJ*(BJ + DN))
  320   TOT2 = TOT2 + TOTJ
        IF(ABS(AJTOT- TOT2)- 0.1*AJTOT) 330,325,325
  325   AJTOT= TOT2
  330   TERM4 = TOT2*TEMP3**N*TEMP1**(.5*DN)
        TERM = TERM1*TERM5*TERM4
        IF (TERM) 390, 450, 390
  390   WRITE(6,50)N,TERM5,K,TERM4,J,TERM
  400   TERMNO = TERMNO + TERM
        GO TO 450
  440   WRITE (6,110)
  450   CN = TEMP4*TERMNO
        CIO = CN*CIC
  500   WRITE(6,20)VO,CIO,TERMNO
        IF(LO)150,150,600
  600   LO=1
        STOP
        END
```

APPENDIX 3

MAGNITUDE OF THE EFFECTIVE PROBE LENGTH CORRECTION

The magnitude of the correction in determining the effective probe length is displayed graphically in Fig. (23) for data from a typical Explorer XVII pass (n_i = 6.4 X 10^5 cm^{-3}, u = 7.9 X 10^5 cm sec^{-1}, T_i = 1000°K, V = 2.7 volts). Curve a represents the total current collected by the probe as a function of the probe aspect. Curve b gives the current collected through the side according to equation (8) without any correction. Curves c, d, e give the same current corrected by using an effective probe length with $\phi = K/r$, $\phi = K/r^2$, and $\phi = K/r^3$ respectively. The corrections are important only at small angles, making the slope of the resulting and end current steeper at these angles. At $\Theta = 0^o$ curves c, d, and e differ from curve b by about 20%, 40% and 50% respectively, and more than half the total current collected is due to the end effect.

APPENDIX 4

TANGENTIAL VELOCITY AT SHEATH EDGE

Since there were no restrictions for collection on the radial and axial velocities, their thermal component in the coordinate system fixed in space was set equal to $\left(\frac{2kT}{3m}\right)^{\frac{1}{2}}$, the component of the most probable thermal velocity along any given direction. However, the tangential velocity was limited by the angular momemtum considerations discussed in Chapter II. Let the thermal component of the tangential velocity by V_t. Then equations (9), (10) and (11) become

$$\dot{r}_a = \left(\frac{2kT}{3m}\right)^{\frac{1}{2}} + u \sin\Theta \cos\zeta_a \tag{58}$$

$$a\dot{\zeta}_a = V_t + u \sin\Theta \sin\zeta_a \tag{59}$$

$$\dot{z}_a = \left(\frac{2kT}{3m}\right)^{\frac{1}{2}} + u \sin\Theta \tag{60}$$

where the subscript a refers to a point on the sheath edge. By the use of equations (58), (59) and (18) and by substituting into equation (17), we get

$$L^2 \leq r_p^2 \left(V_t^2 + 2V_t u \sin\Theta \sin\zeta_a + y\right) \tag{61}$$

where

$$y = u^2\sin^2\Theta + \frac{2kT}{3m} + 2\left(\frac{2kT}{3m}\right)^{\frac{1}{2}} u \sin\Theta \cos\zeta_a + 2\phi/m$$

But by equations (59) and (18), we have

$$L^2 = a^2 \left(V_t^2 + 2V_t u \sin\Theta \sin\zeta_a + u^2\sin^2\Theta \sin^2\zeta_a\right) \tag{62}$$

Combining equation (61) and (62), we get

$$\left(V_t\right)_{max} = - u \sin \Theta \sin \zeta_a \pm y^{\frac{1}{2}} r_{p/a}$$

where the subscript refers to the maximum allowed value. Then the maximum value of $a\dot{\zeta}_o$ is

$$(a \dot{\zeta}_a)_{max} = (V_t)_{max} + u \sin \Theta \sin \zeta_a$$

$$= \pm y^{\frac{1}{2}} r_{p/a} \qquad (63)$$

Equation (63) shows that $(a \dot{\zeta}_a)_{max}$ is the same in either direction.

To find an average value for V_t, we should integrate the velocity distribution between 0 and $(V_t)_{max}$. However, we can make an approximation by considering the most probable thermal velocity in the direction opposite to the drift velocity. Since $\left(\frac{2kT}{3m}\right)^{\frac{1}{2}}$ and $u \sin \Theta \sin \zeta_a$ are of the same order between $250^{\circ}K$ and $2000^{\circ}K$, we can find a value of ζ_a for which $\left(\frac{2kT}{3m}\right)^{\frac{1}{2}} - u \sin \Theta \sin \zeta_a < (a\dot{\zeta}_a)_{max}$. In particular, we can find a value of ζ_a for which

$$\left(\frac{2kT}{3m}\right)^{\frac{1}{2}} - u \sin \Theta \sin \zeta_a = 0.5(a\dot{\zeta}_a)_{max}$$

In effect we consider that the majority of particles collected are those with the most probable thermal velocity in the direction opposite to the drift velocity. Particles with the most probable thermal velocity in the same direction as the drift velocity would not be collected since $\left(\frac{2kT}{3m}\right)^{\frac{1}{2}} > \left(a\dot{\zeta}_a\right)_{max}$ for $T > 250^{\circ}$. The value of $0.5\ (a\dot{\zeta}_a)_{max}$ was arbitrarily chosen for the tangential velocity. However the arbitrary nature of the factor of 0.5 was offset by the fact

that any particuler choice of a factor less than 1 did not appreciably change the value of the radial velocity (less than 2%), which together with the axial velocity was the dominant velocity term in the determination of the effective probe length. Thus the equations used to determine the tangential velocity at the sheath edge were

$$a\dot{\zeta}_a = 0.5(a\dot{\zeta}_a)_{max} \tag{52}$$

$$a\dot{\zeta}_a = \left(\frac{2kT}{3m}\right)^{\frac{1}{2}} - u \sin\Theta \sin\zeta_a \tag{53}$$

$$(a\dot{\zeta}_a)_{max} = (r_p/a)\left[\frac{2kT}{3m} + 2\left(\frac{2kT}{3m}\right)^{\frac{1}{2}} u \sin\Theta \cos\zeta_a + 2\phi/m + u^2\sin^2\Theta\right]^{\frac{1}{2}} \tag{54}$$

REFERENCES CITED

Aitkin, A. C., and S. J. Bauer, "The Ionosphere," in Introduction to Space Science, edited by W. N. Hess, pp. 133-164, Gordon and Breach Science Publishers, New York, 1965.

Bettinger, R. T., "Wing-Slope Techniques for the Analysis of Langmuir Probe Characteristics," Dept. of Phys. and Astron. Tech. Report 484, 1965.

Bettinger, R. T., "An End Effect Associated with Cylindrical Langmuir Probes Moving at Satellite Velocities," Dept. of Phys. and Astron. Tech. Report 566, 1966.

Bettinger, R. T., and E. H. Walker, "Relationship for Plasma Sheaths about Langmuir Probes," Phys. Fluids, v. 8, pp. 748-751, 1965.

Bordeau, R. E., and S. J. Bauer, "Structure of the Upper Atmosphere Deduced from Charged Particle Measurements on Rockets and the Explorer VIII Satellite," in Space Research III, edited by W. Priester, pp. 173-192, North Holland, Amsterdam, 1963.

Brace, L. H., and N. W. Spencer, "Detailed Behavior of the Midlatitude Ionosphere from the Explorer XVII Satellite," Planet. Space Sci., v. 13, pp. 647-665, 1965.

Dalgarno, A., M. B. McElroy and R. J. Moffett, "Electron Temperatures in the Ionosphere," Planet. Space Sci., v. 11, pp. 463-483, 1963.

Evans, J. V., and M. Loewenthal, "Ionospheric Backscatter Observations," Planet. Space Sci., v. 12, pp. 915-943, 1964.

Hanson, W. B., "Electron Temperatures in the Upper Atmosphere," in Space Research III, edited by W. Priester, pp. 282-302, 1963.

Istomin, V.G., "An Investigation of the Ionic Composition of the Earth's Atmosphere Using Rockets and Satellites," in Artificial Earth Satellites, edited by L. V. Kuynosova, pp. 40-44, Plenum Press, New York, 1960.

Istomin, V. G., and A. A. Pokhunkov, "Mass-Spectrometer Measurements of Atmospheric Composition in the USSR," in Space Research III, edited by W. Priester, pp. 117-130, North Holland, Amsterdam, 1963.

Kanal, M., "Theory of Current Collection of Moving Cylindrical Probes," Phys. Rev., v. 35, pp. 1697-1703, 1964.

Mott-Smith, H. M., and I. Langmuir, "The Theory of Collectors in Gaseous Discharges," Phys. Rev., v. 28, pp. 727-763, 1926.

Newton, G. P., R. Horowitz and W. Priester, "Atmospheric Density and Temperature Variations from the Explorer XVII Satellite and a Further Comparison with Satellite Drag," Planet. Space Sci., v. 13, pp.599-616, 1965.

Spencer, N. W., "The Explorer XVII Satellite," Planet. Space Sci., v. 13, pp. 593-598, 1965.

Spencer, N. W., L. H. Brace, G. R. Carigan, D. R. Taeusch, and H. Niemann, "Electron and Molecular Nitrogen Temperature and Density in the Thermosphere," J. Geophys. Res., v. 70, pp. 2665-2698, 1965.

Walker, E. H., "Plasma Sheath and Screening Around a Stationary Charged Sphere and a Rapidly Moving Charged Body," in Interactions of Space Vehicles with an Ionized Atmosphere, edited by S. F. Singer, pp. 82-87, Pergamon Press, Oxford, 1965.

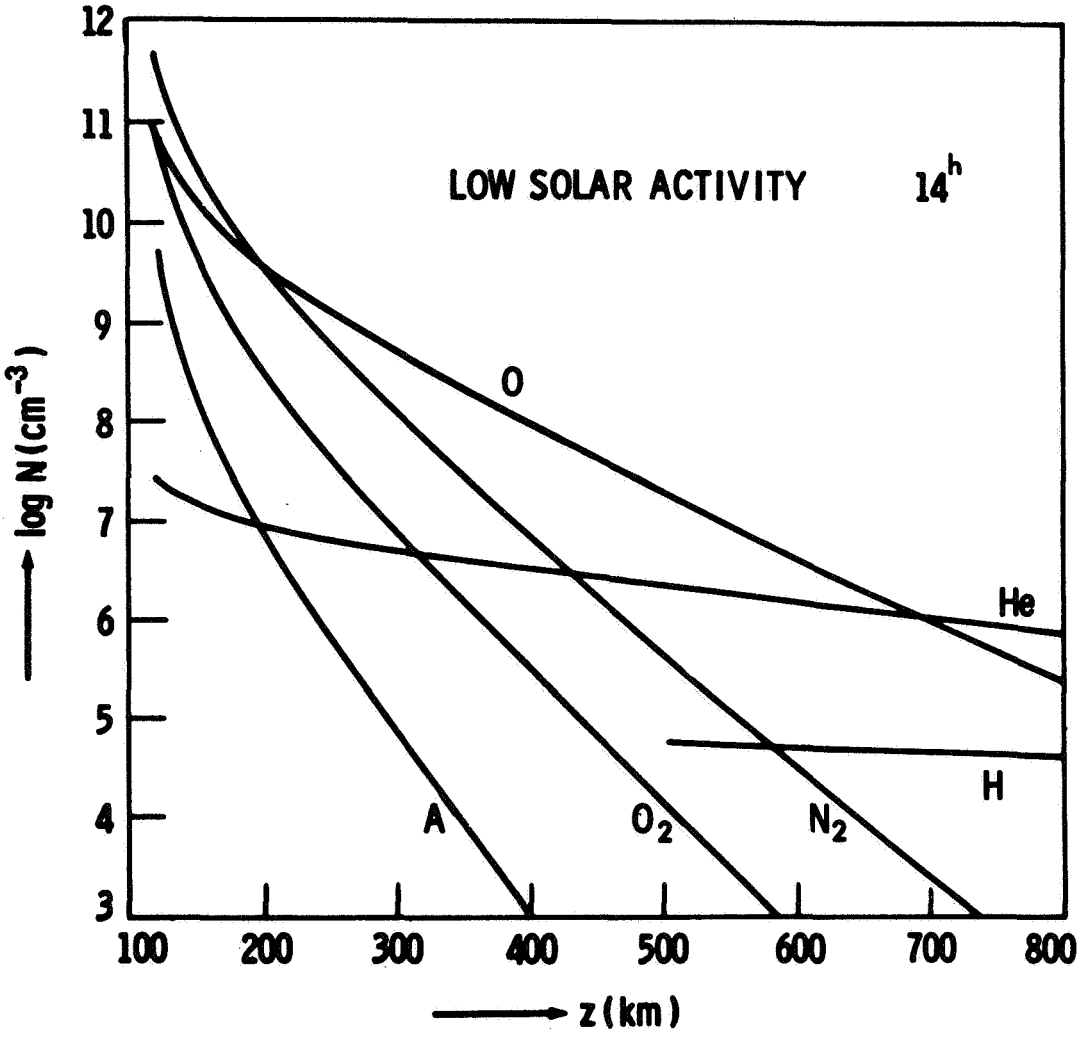
LOW SOLAR ACTIVITY
14h
O
He
H
A
O2
N2
log N(cm-3)
z(km)
12
11
10
9
8
7
6
5
4
3
100
200
300
400
500
600
700
800

FIG. 1

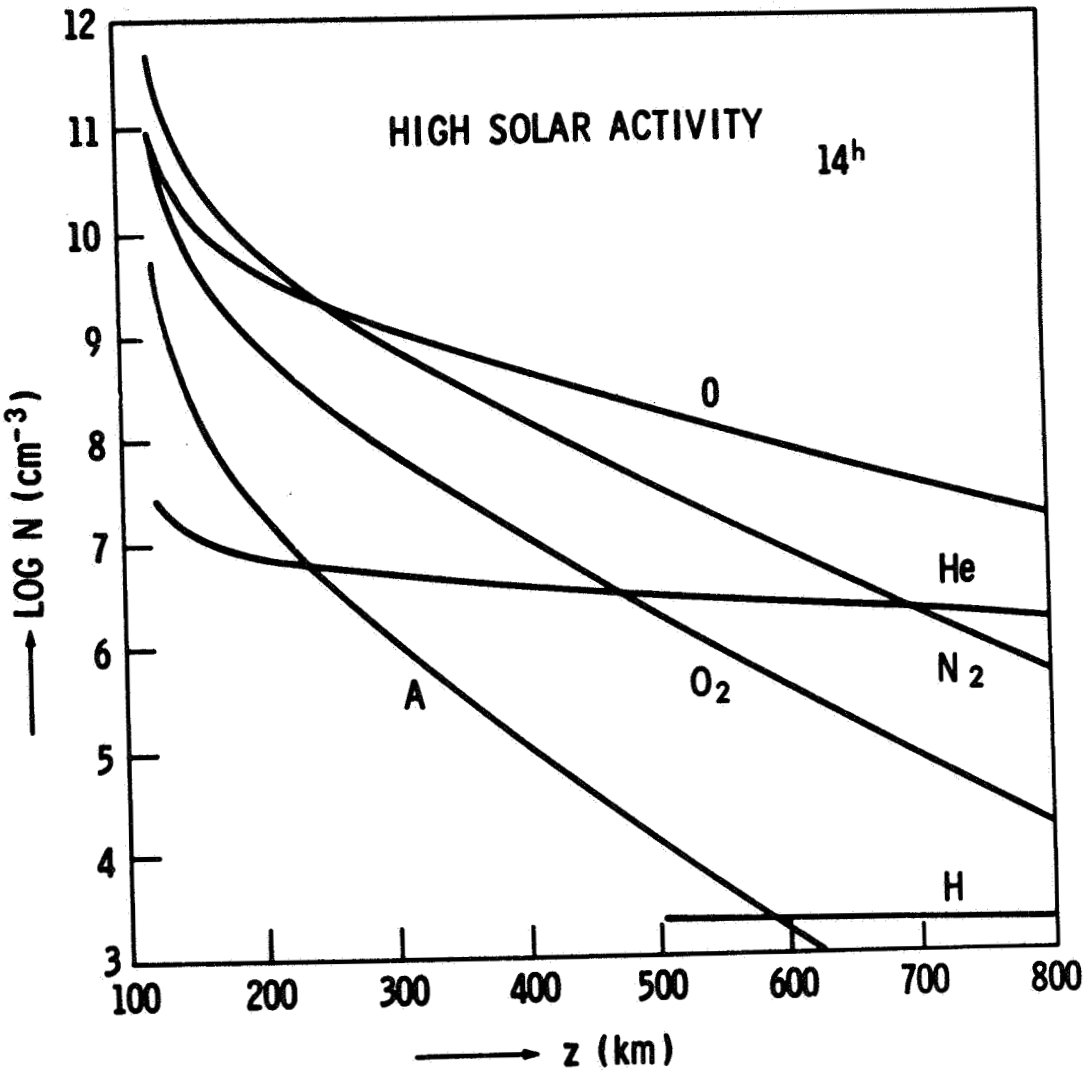
HIGH SOLAR ACTIVITY
14h
O
He
N2
O2
A
H
LOG N (cm-3)
z (km)
12
11
10
9
8
7
6
5
4
3
100
200
300
400
500
600
700
800

FIG. 2

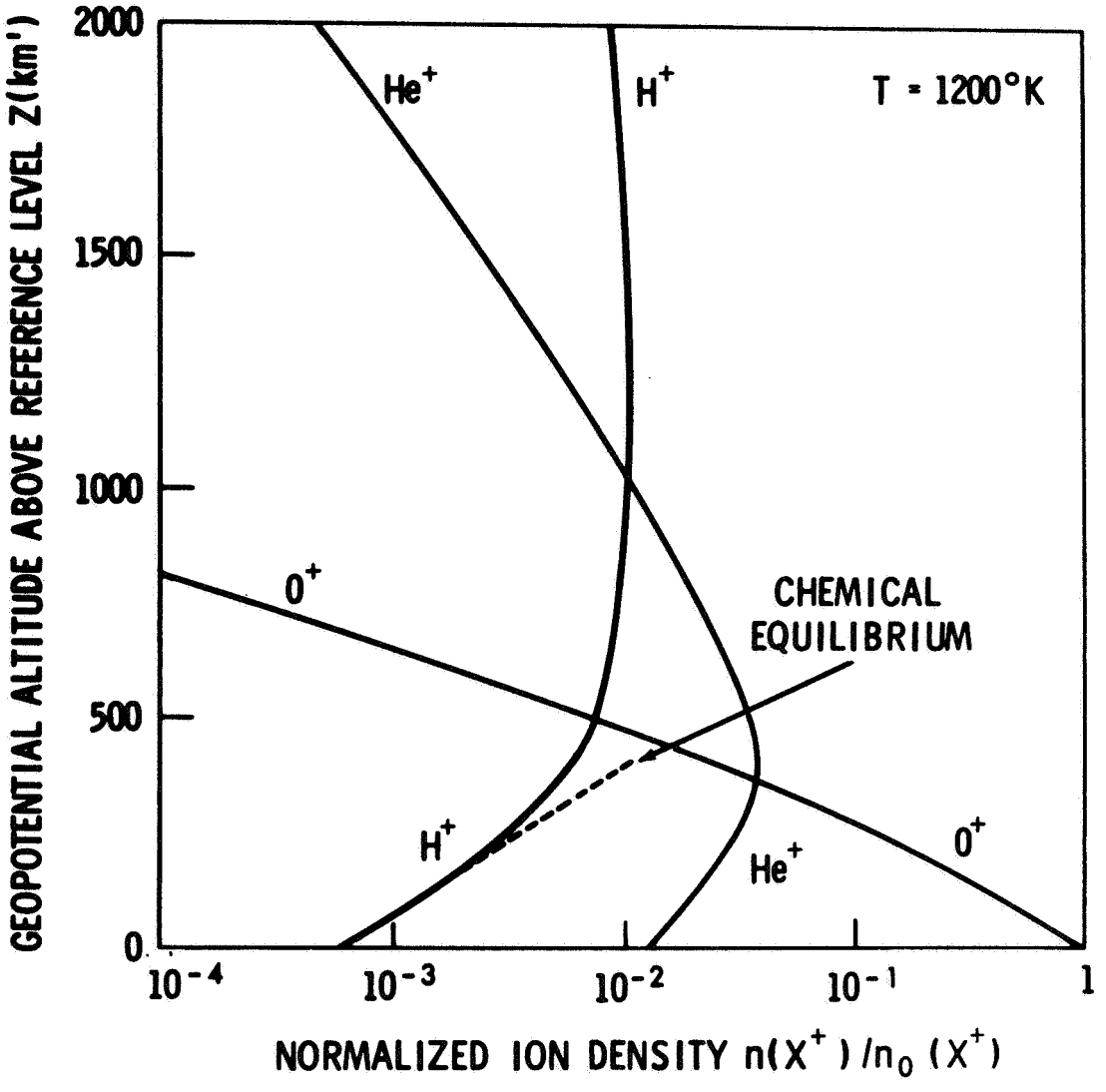
GEOPOTENTIAL ALTITUDE ABOVE REFERENCE LEVEL Z(km')
2000
1500
1000
500
0
He+
H+
T = 1200°K
O+
CHEMICAL
EQUILIBRIUM
H+
He+
O+
10-4
10-3
10-2
10-1
1
NORMALIZED ION DENSITY n(X+) /n0 (X+)

FIG. 3

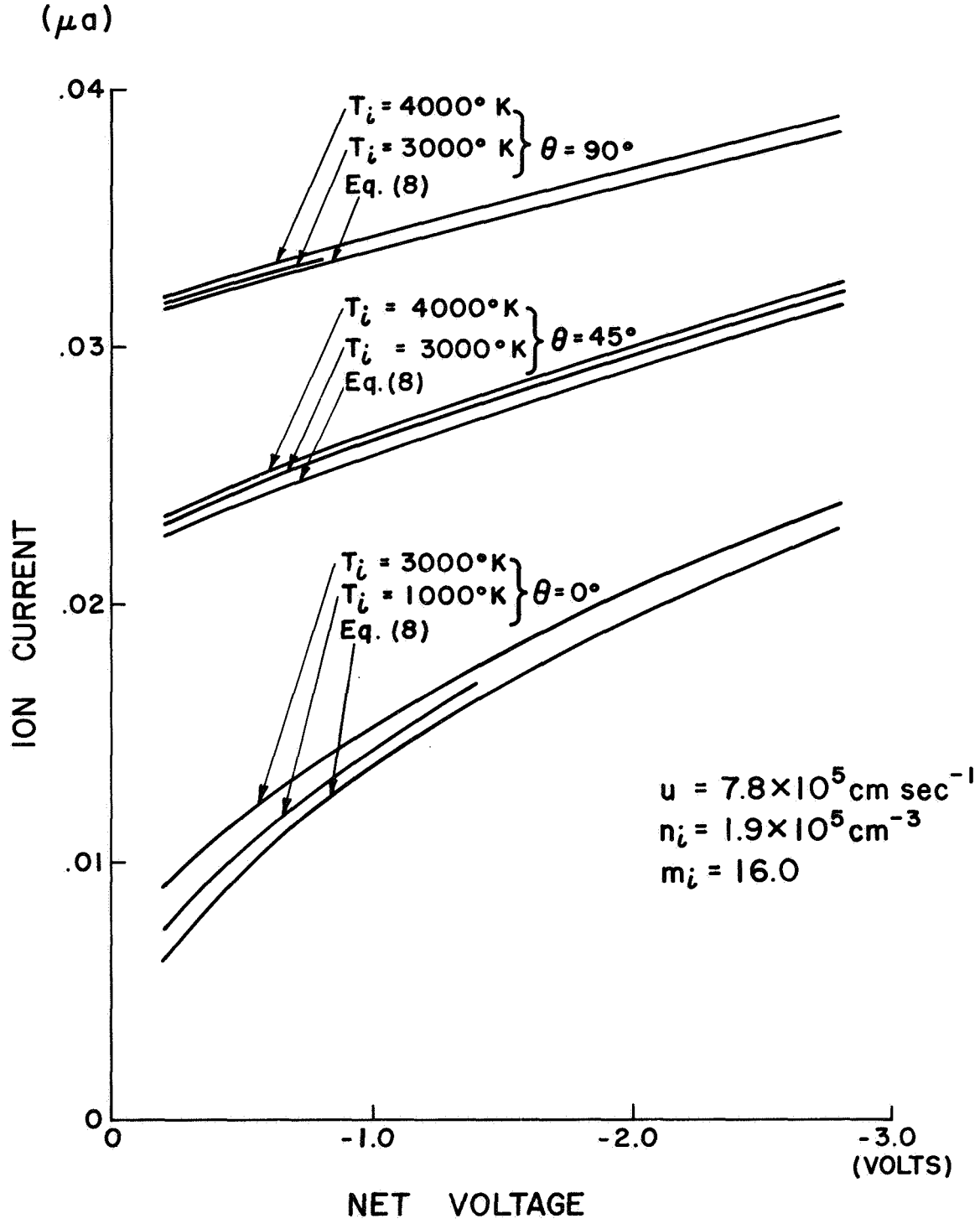
(μa)
.04
.03
.02
.01
0
ION CURRENT
T_i = 4000° K
T_i = 3000° K
θ = 90°
Eq. (8)
T_i = 4000° K
T_i = 3000° K
θ = 45°
Eq. (8)
T_i = 3000° K
T_i = 1000° K
θ = 0°
Eq. (8)
u = 7.8×10⁵cm sec⁻¹
n_i = 1.9×10⁵cm⁻³
m_i = 16.0
0
-1.0
-2.0
-3.0
(VOLTS)
NET VOLTAGE

FIG. 4

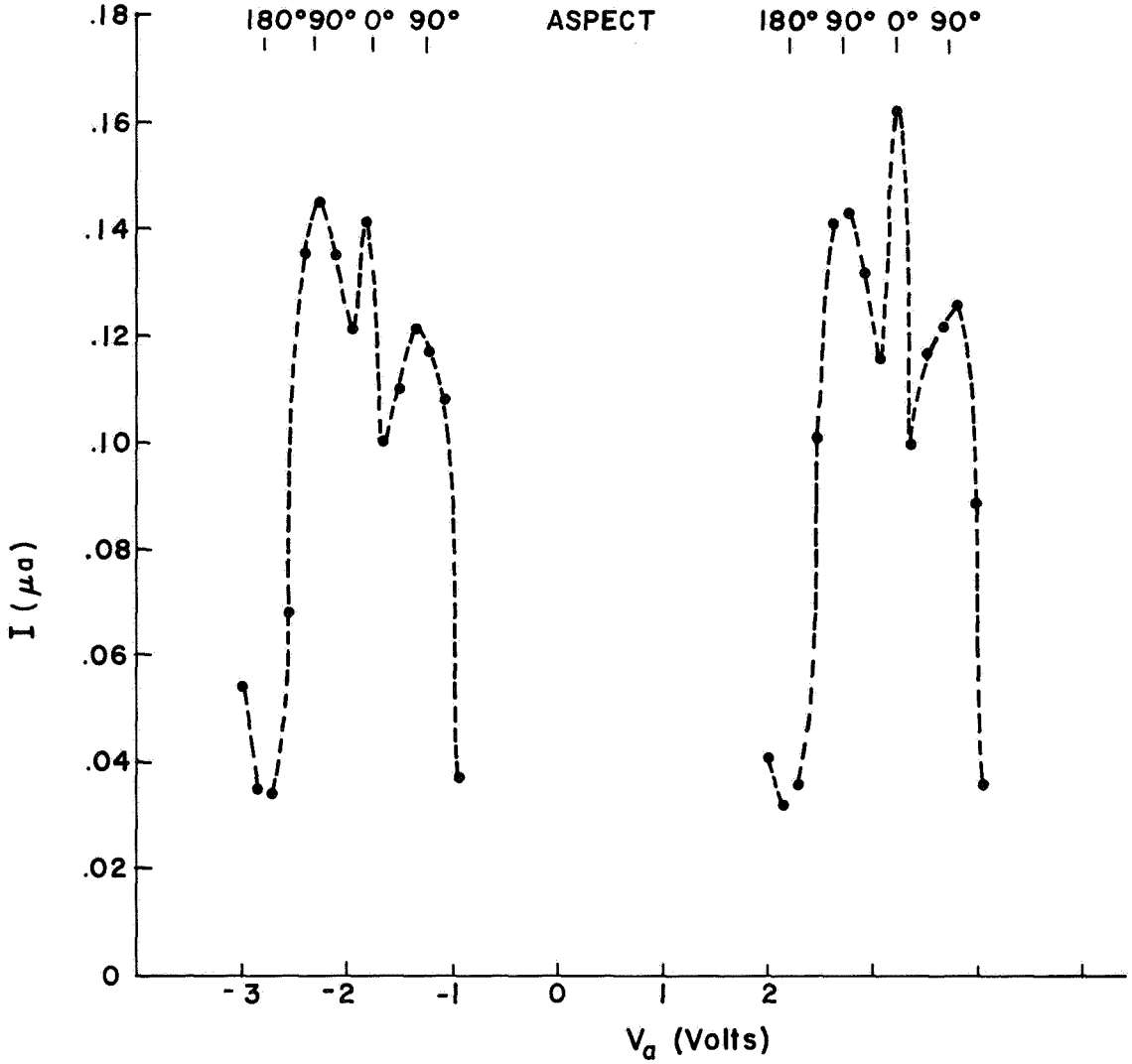
.18
.16
.14
.12
.10
.08
.06
.04
.02
0
I (μa)
180° 90° 0° 90°
ASPECT
180° 90° 0° 90°
-3
-2
-1
0
1
2
V_a (Volts)

FIG. 5.

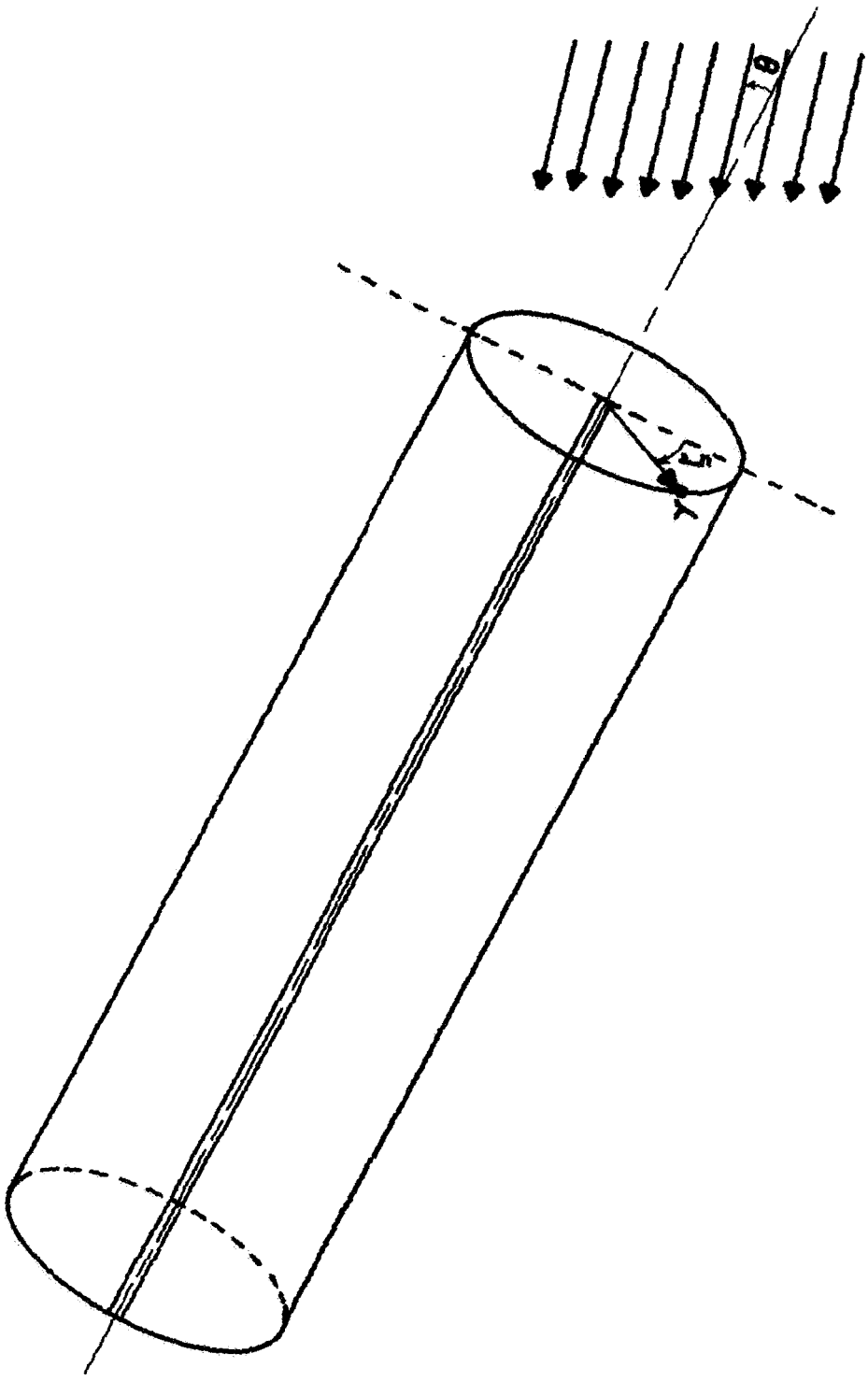

FIG. 6

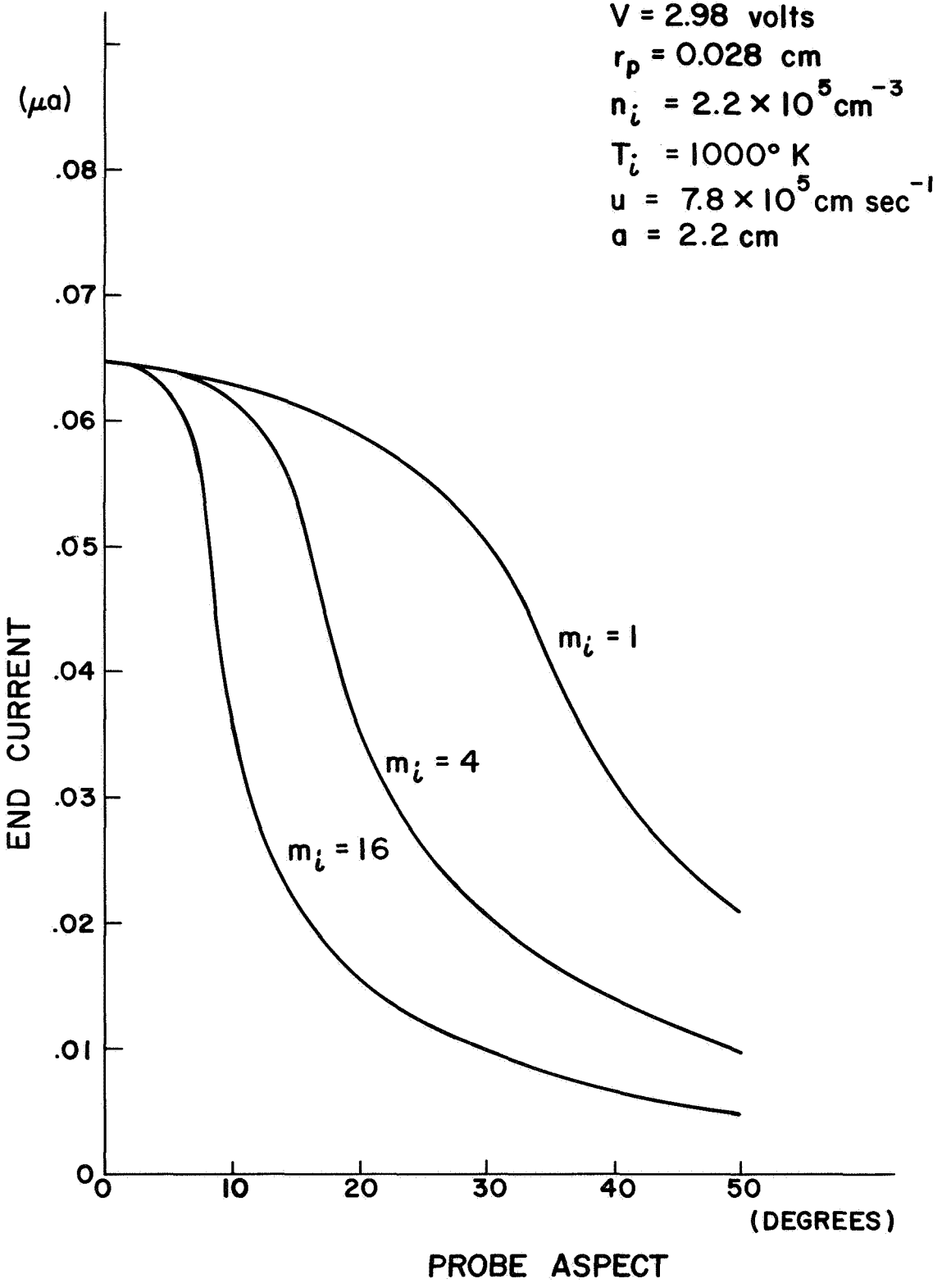
V = 2.98 volts
r_p = 0.028 cm
n_i = 2.2 × 10^{5}cm^{-3}
T_i = 1000° K
u = 7.8 × 10^{5}cm sec^{-1}
a = 2.2 cm
(μa)
.08
.07
.06
.05
.04
.03
.02
.01
0
END CURRENT
m_i = 1
m_i = 4
m_i = 16
0
10
20
30
40
50
(DEGREES)
PROBE ASPECT

FIG. 7

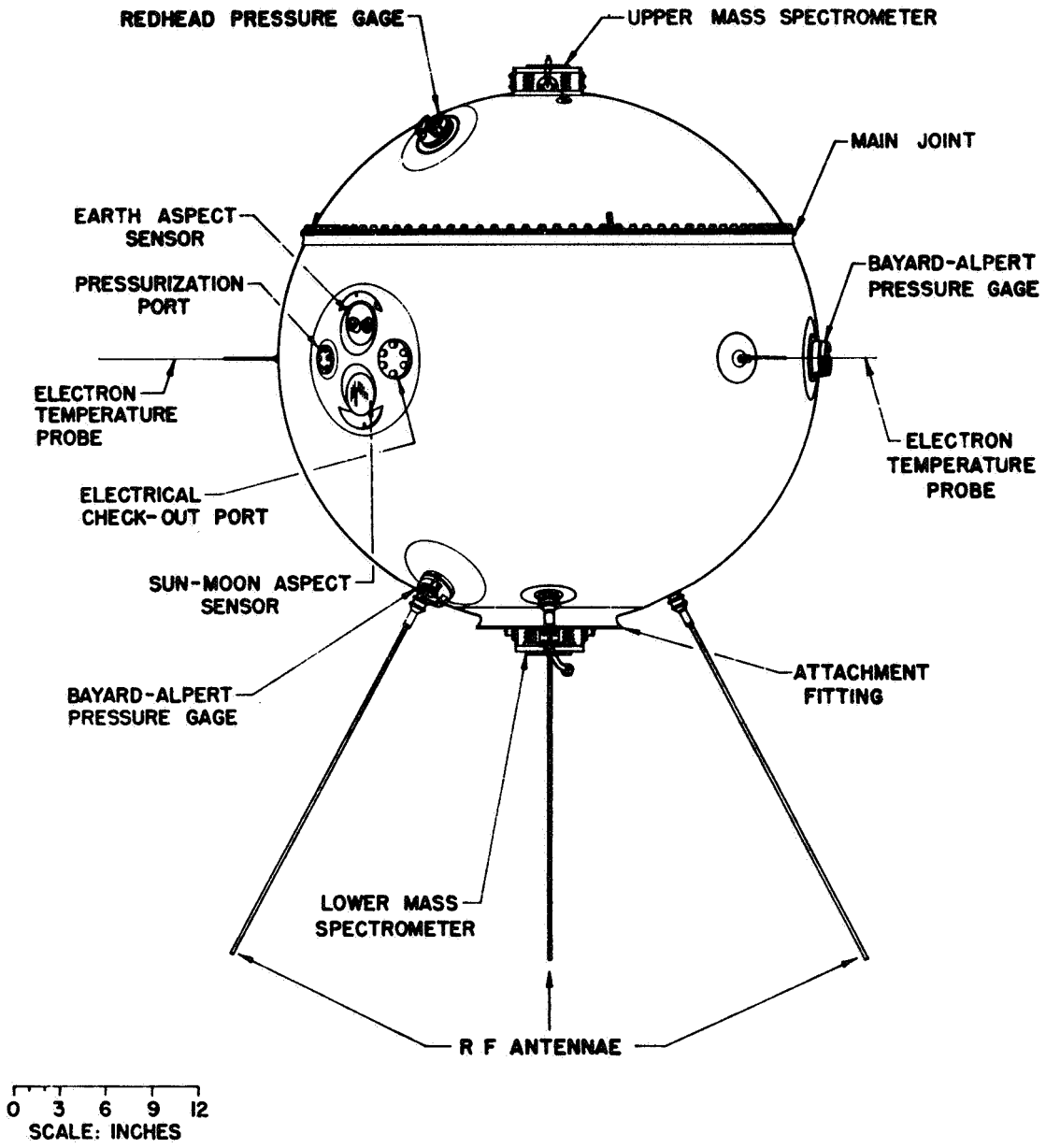
REDHEAD PRESSURE GAGE
UPPER MASS SPECTROMETER
MAIN JOINT
EARTH ASPECT SENSOR
PRESSURIZATION PORT
BAYARD-ALPERT PRESSURE GAGE
ELECTRON TEMPERATURE PROBE
ELECTRON TEMPERATURE PROBE
ELECTRICAL CHECK-OUT PORT
SUN-MOON ASPECT SENSOR
ATTACHMENT FITTING
BAYARD-ALPERT PRESSURE GAGE
LOWER MASS SPECTROMETER
R F ANTENNAE
0 3 6 9 12
SCALE: INCHES

FIG. 8

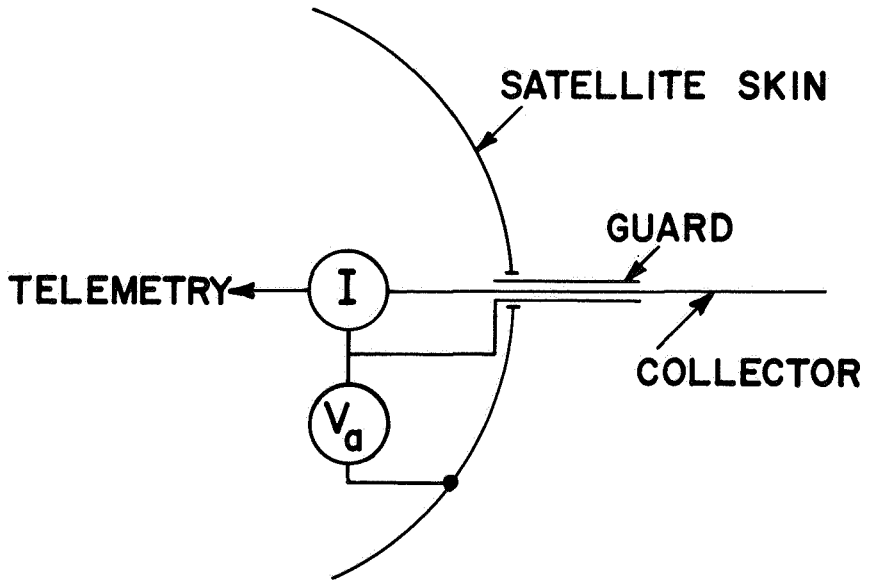

FIG. 9.

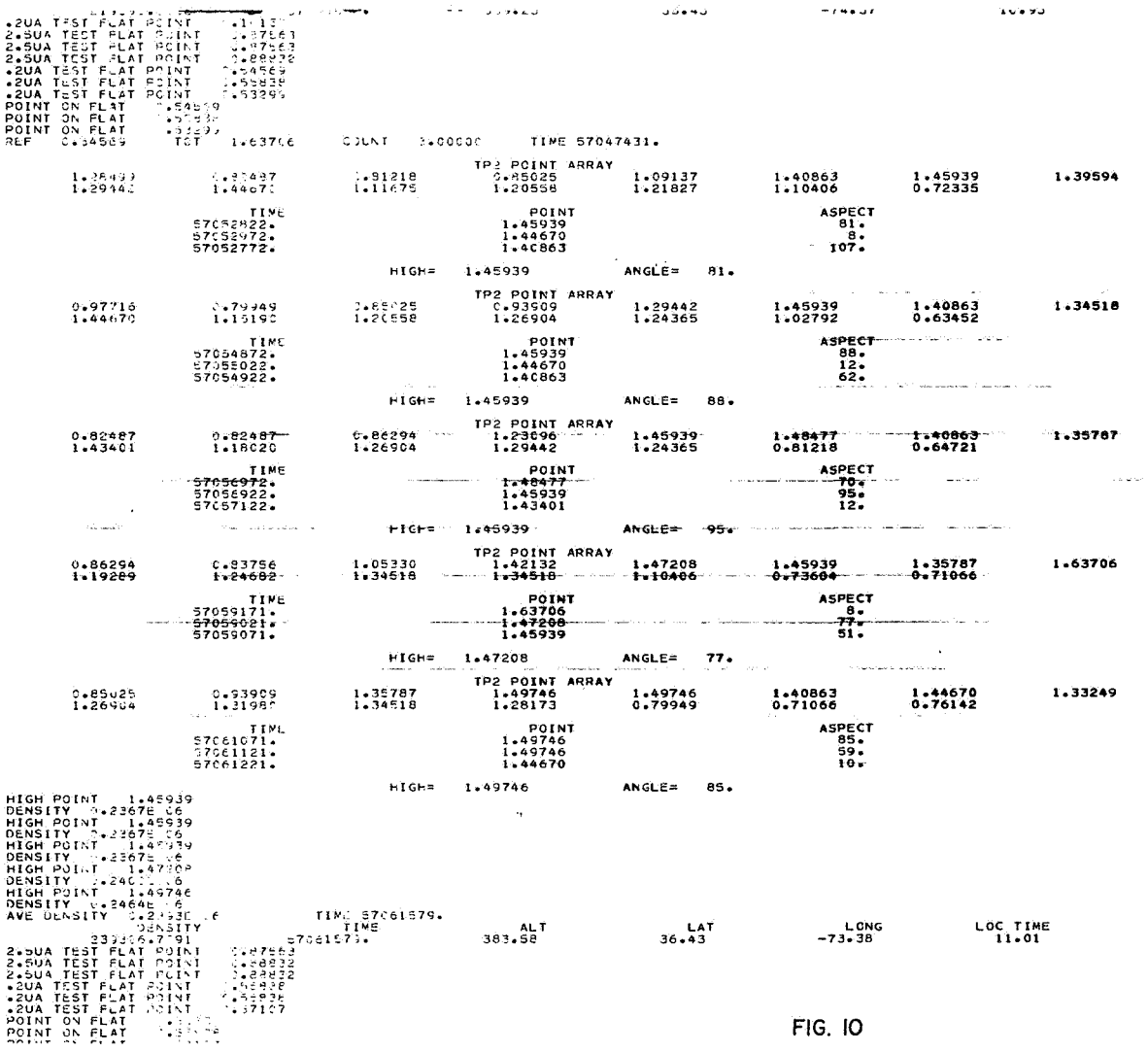
•2UA TEST FLAT POINT
2.5UA TEST FLAT POINT
2.5UA TEST FLAT POINT
2.5UA TEST FLAT POINT
•2UA TEST FLAT POINT
•2UA TEST FLAT POINT
•2UA TEST FLAT POINT
POINT ON FLAT
POINT ON FLAT
POINT ON FLAT
REF 0.84569 TGT 1.63706 COUNT 0.00000 TIME 57047431.
TP2 POINT ARRAY
1.26499 0.82487 0.91218 0.85025 1.09137 1.40863 1.45939 1.39594
1.29442 1.44670 1.11675 1.20558 1.21827 1.10406 0.72335
TIME POINT ASPECT
57052822. 1.45939 81.
57052972. 1.44670 8.
57052772. 1.40863 107.
HIGH= 1.45939 ANGLE= 81.
TP2 POINT ARRAY
0.97716 0.79949 0.85025 0.93909 1.29442 1.45939 1.40863 1.34518
1.44670 1.15190 1.20558 1.26904 1.24365 1.02792 0.63452
TIME POINT ASPECT
57054872. 1.45939 88.
57055022. 1.44670 12.
57054922. 1.40863 62.
HIGH= 1.45939 ANGLE= 88.
TP2 POINT ARRAY
0.82487 0.82487 0.86294 1.23696 1.45939 1.48477 1.40863 1.35787
1.43401 1.18620 1.26904 1.29442 1.24365 0.81218 0.64721
TIME POINT ASPECT
57056972. 1.48477 70.
57056922. 1.45939 95.
57057122. 1.43401 12.
HIGH= 1.45939 ANGLE= 95.
TP2 POINT ARRAY
0.86294 0.83756 1.05330 1.42132 1.47208 1.45939 1.35787 1.63706
1.19289 1.24682 1.34518 1.34518 1.10406 0.73604 0.71066
TIME POINT ASPECT
57059171. 1.63706 8.
57059021. 1.47208 77.
57059071. 1.45939 51.
HIGH= 1.47208 ANGLE= 77.
TP2 POINT ARRAY
0.85025 0.93909 1.35787 1.49746 1.49746 1.40863 1.44670 1.33249
1.26904 1.31985 1.34518 1.28173 0.79949 0.71066 0.76142
TIME POINT ASPECT
57061071. 1.49746 85.
57061121. 1.49746 59.
57061221. 1.44670 10.
HIGH= 1.49746 ANGLE= 85.
HIGH POINT 1.45939
DENSITY
HIGH POINT 1.45939
DENSITY
HIGH POINT 1.45939
DENSITY
HIGH POINT 1.47208
DENSITY
HIGH POINT 1.49746
DENSITY
AVE DENSITY TIME 57061579.
DENSITY TIME ALT LAT LONG LOC TIME
57061579. 383.58 36.43 -73.38 11.01
2.5UA TEST FLAT POINT
2.5UA TEST FLAT POINT
2.5UA TEST FLAT POINT
•2UA TEST FLAT POINT
•2UA TEST FLAT POINT
•2UA TEST FLAT POINT
POINT ON FLAT
POINT ON FLAT

FIG. 10

TIME OF MAX RAM	LATITUDE	ALTITUDE	LOCAL TIME	LONGITUDE
56980.592	33.42	400.82	10.80	-76.27

ANGLE BETWEEN SENSOR AND VELOCITY VECTOR IS 32. AT START, AND 25. AT END OF CURVE PASS 472.

S6 DATA CURVE

TIME	TEMP	SAT FLAG	1=1UA	CHANNEL SPACE	FIRST CHANNEL	REF
56990855.	4357.	3.	0	556	18	96.

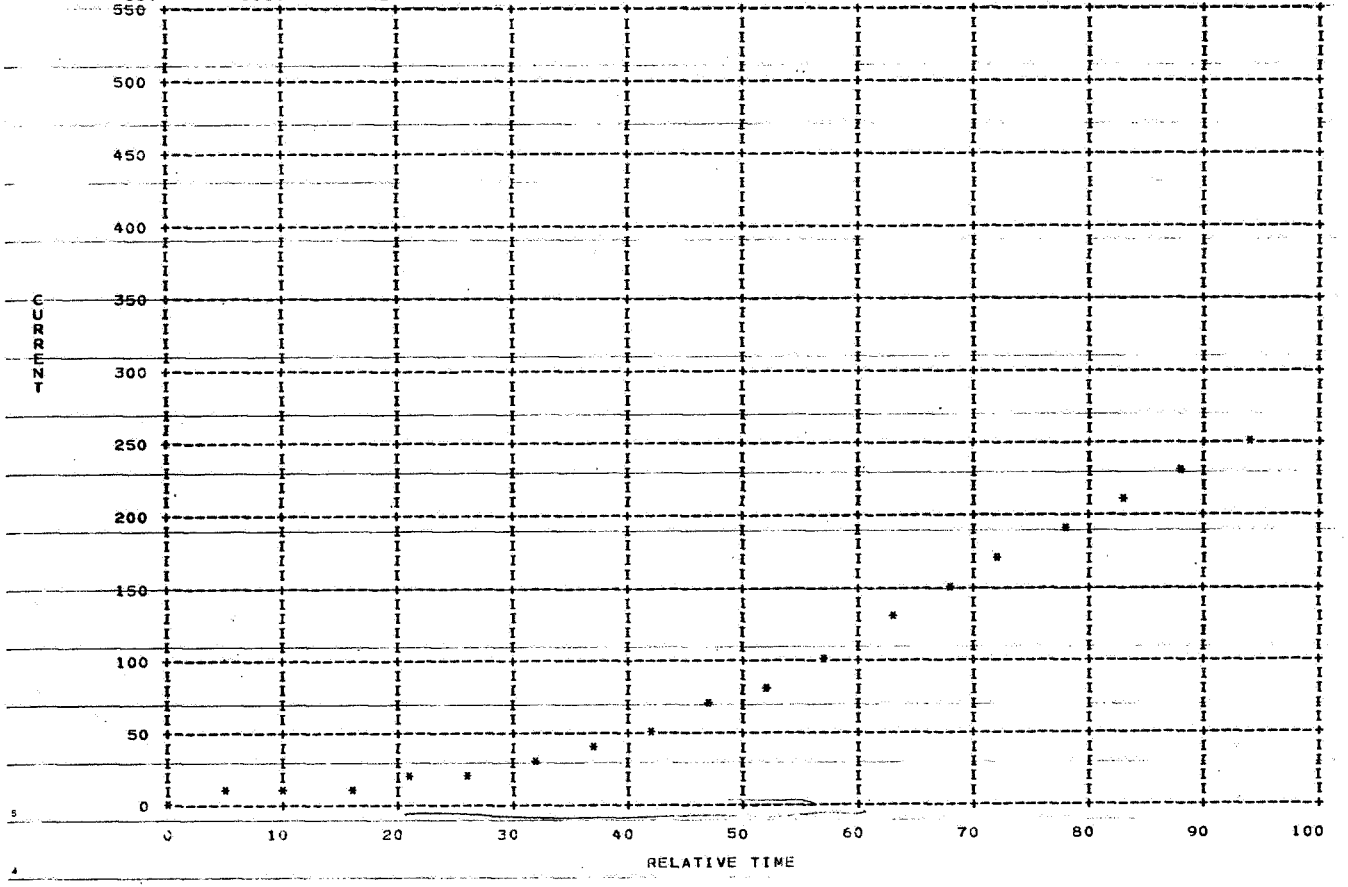

FIG. 11

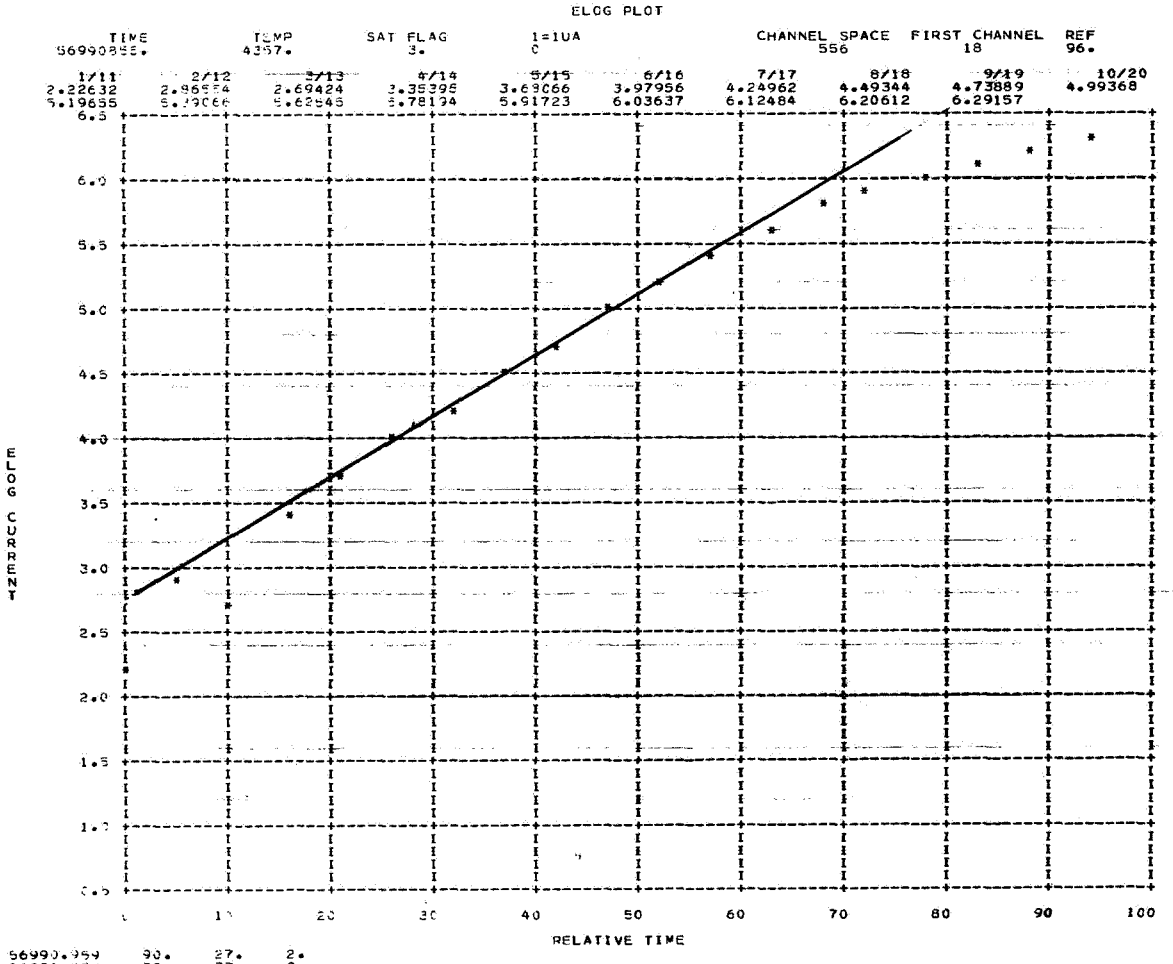


```
56990.959     90.     27.     2.
56991.059     90.     77.     2.
MAIN  CALOW=          97.72AK=          96.CCYINPUT(2)=         104.06
                                56990960.  CANNOT MAKE PRELIMINARY TEMP DETERMINATION
MAIN  CALOW=          97.72AK=          96.CCYINPUT(2)=         104.06
56991.071     90.     78.     2.
56991.171     90.    134.     1.
MAIN  CALOW=          97.72AK=          96.CCYINPUT(2)=         104.06
TEMP((NSTOP-2),(NSTOP-6))=      3328.     AK=     96.
TPI   CALOW=          97.72AK=          96.CCYINPUT(2)=         104.06
FINAL AK=       96.FINAL TEMP=      3328.FINAL SLOPE=       0.06053
TPI   CALOW=          97.72AK=          96.CCYINPUT(2)=         104.06
```

FIG. 12

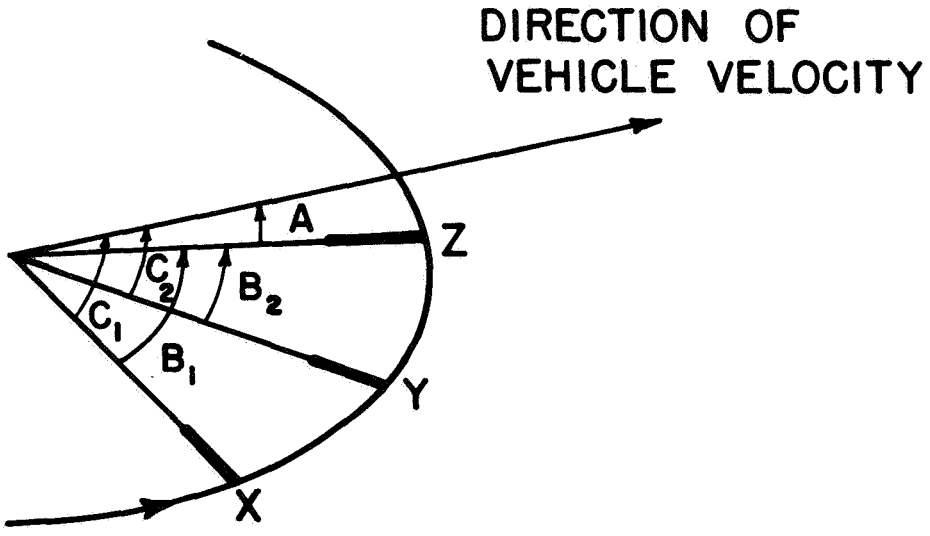

FIG. 13.

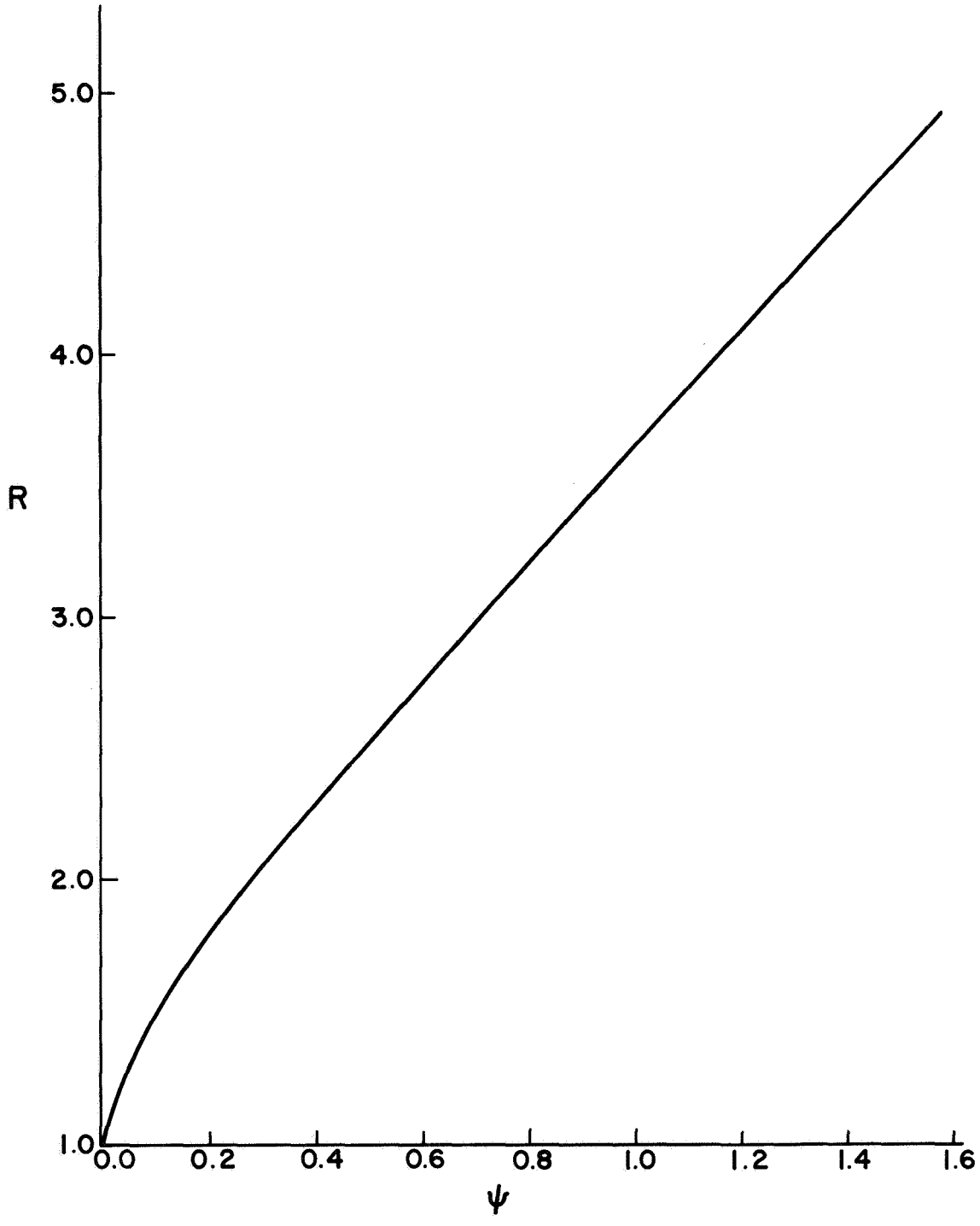

FIG. 14.

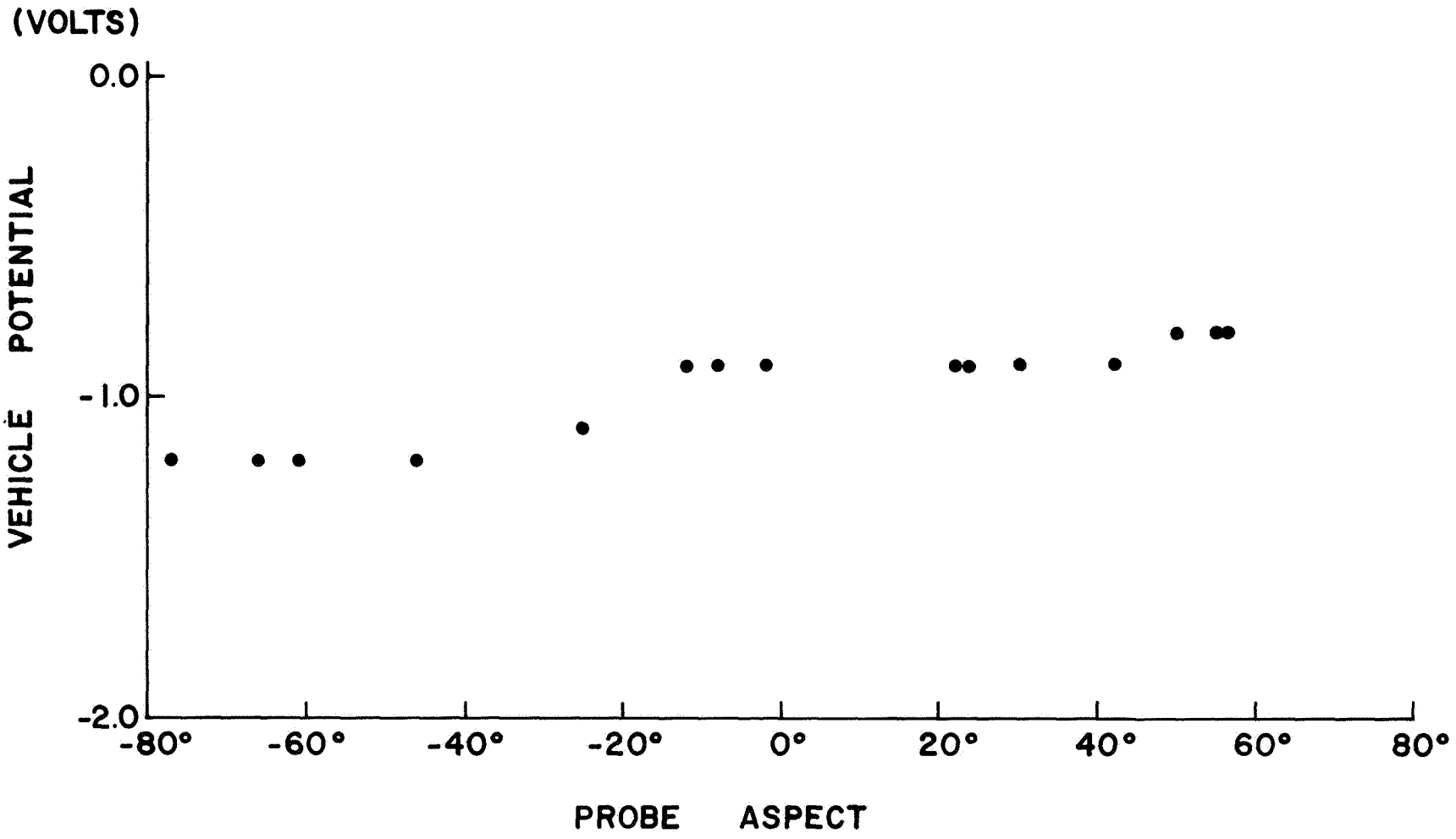
(VOLTS)
0.0
-1.0
-2.0
VEHICLE POTENTIAL
-80°
-60°
-40°
-20°
0°
20°
40°
60°
80°
PROBE ASPECT

FIG. 15.

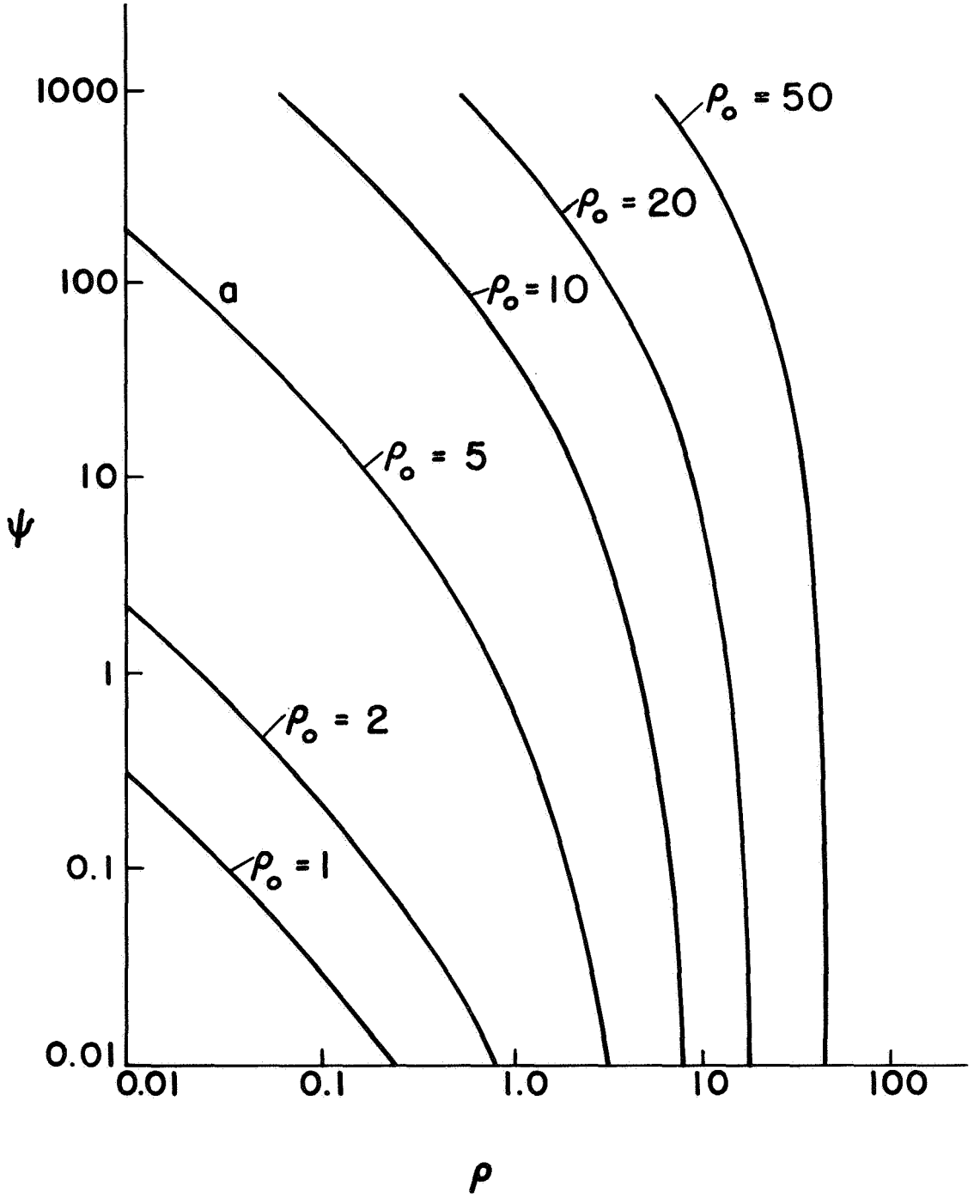
1000
100
10
1
0.1
0.01
ψ
0.01
0.1
1.0
10
100
ρ
a
$\rho_o = 50$
$\rho_o = 20$
$\rho_o = 10$
$\rho_o = 5$
$\rho_o = 2$
$\rho_o = 1$

FIG. 16.

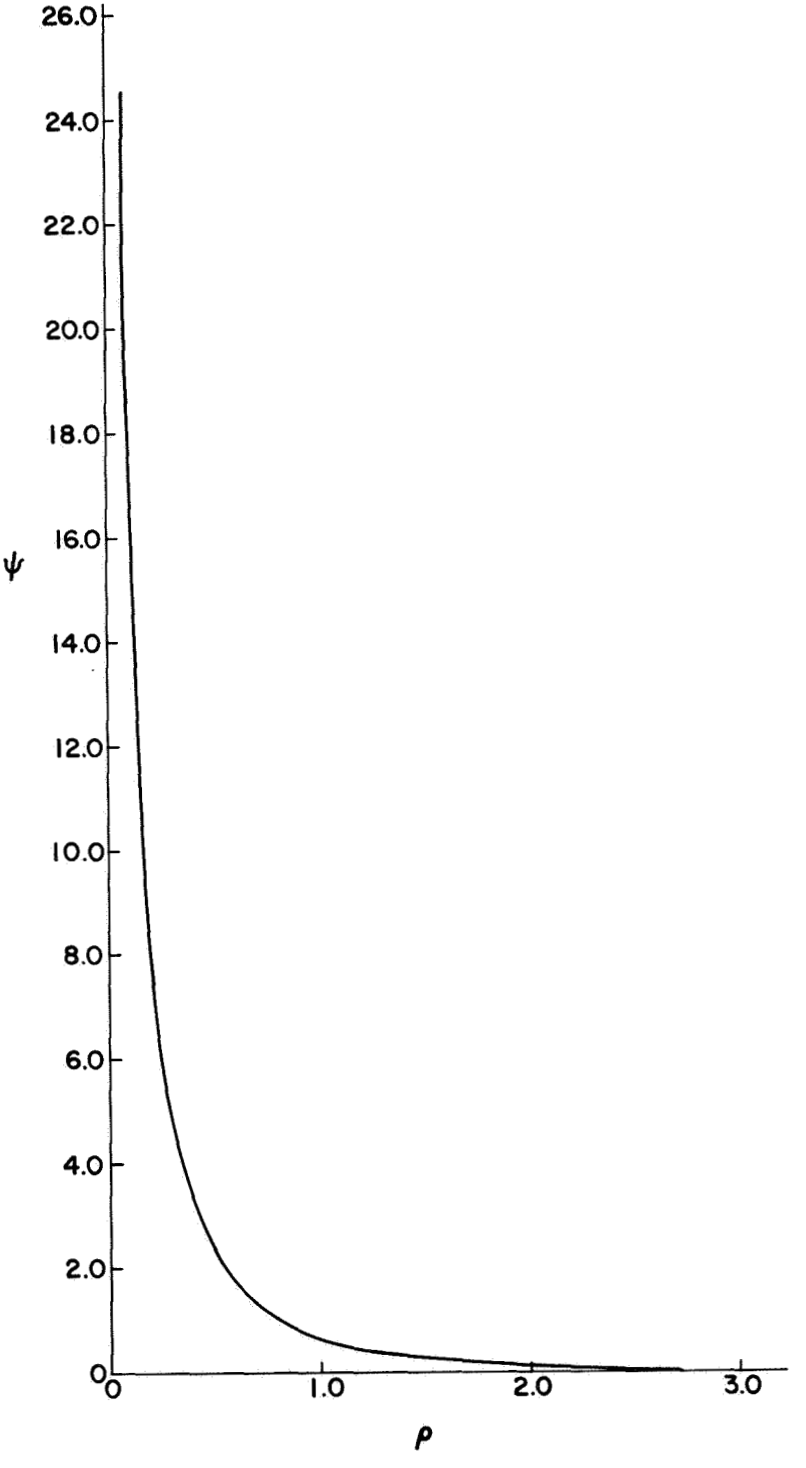

FIG. 17

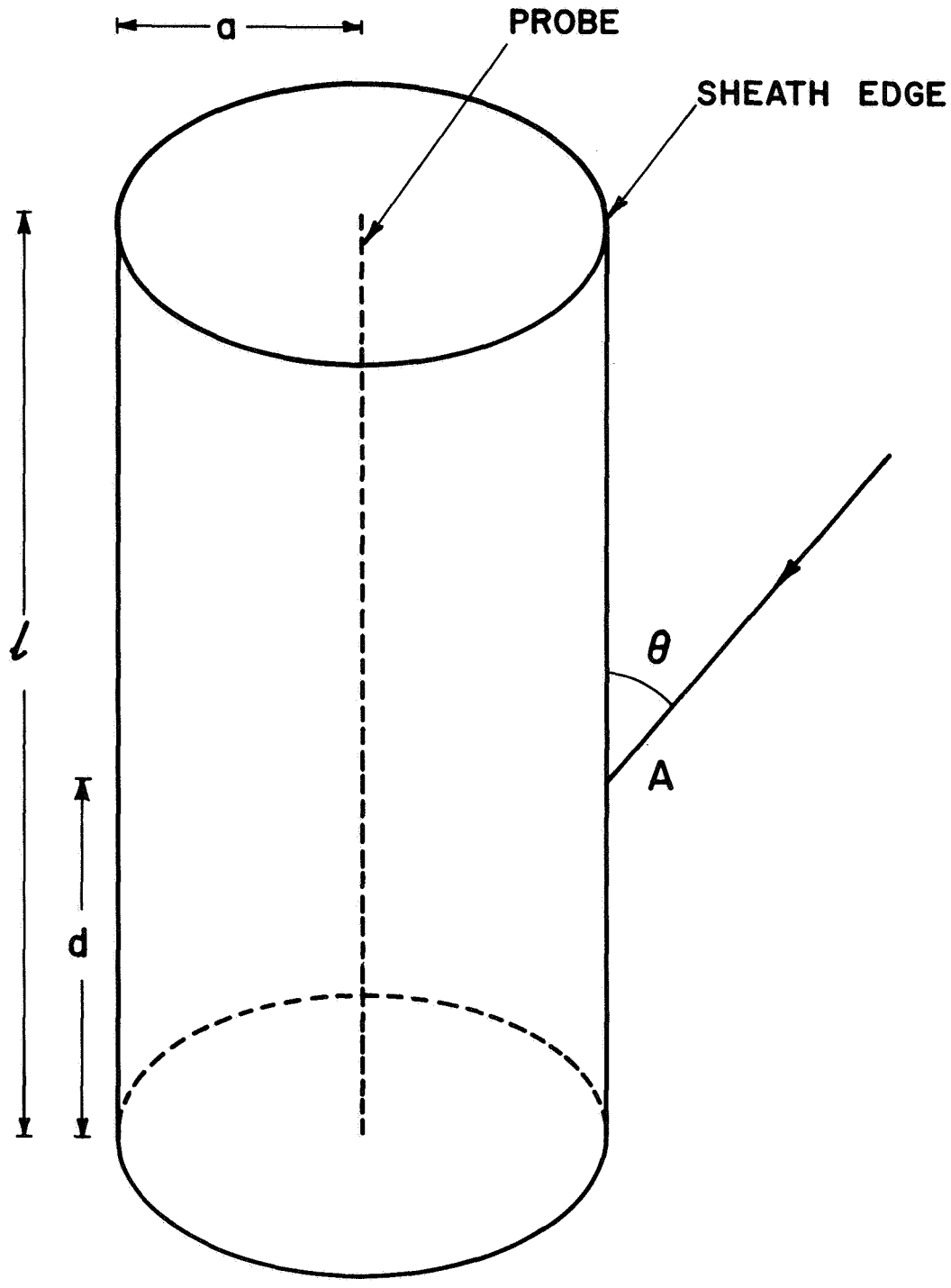

FIG. 18.

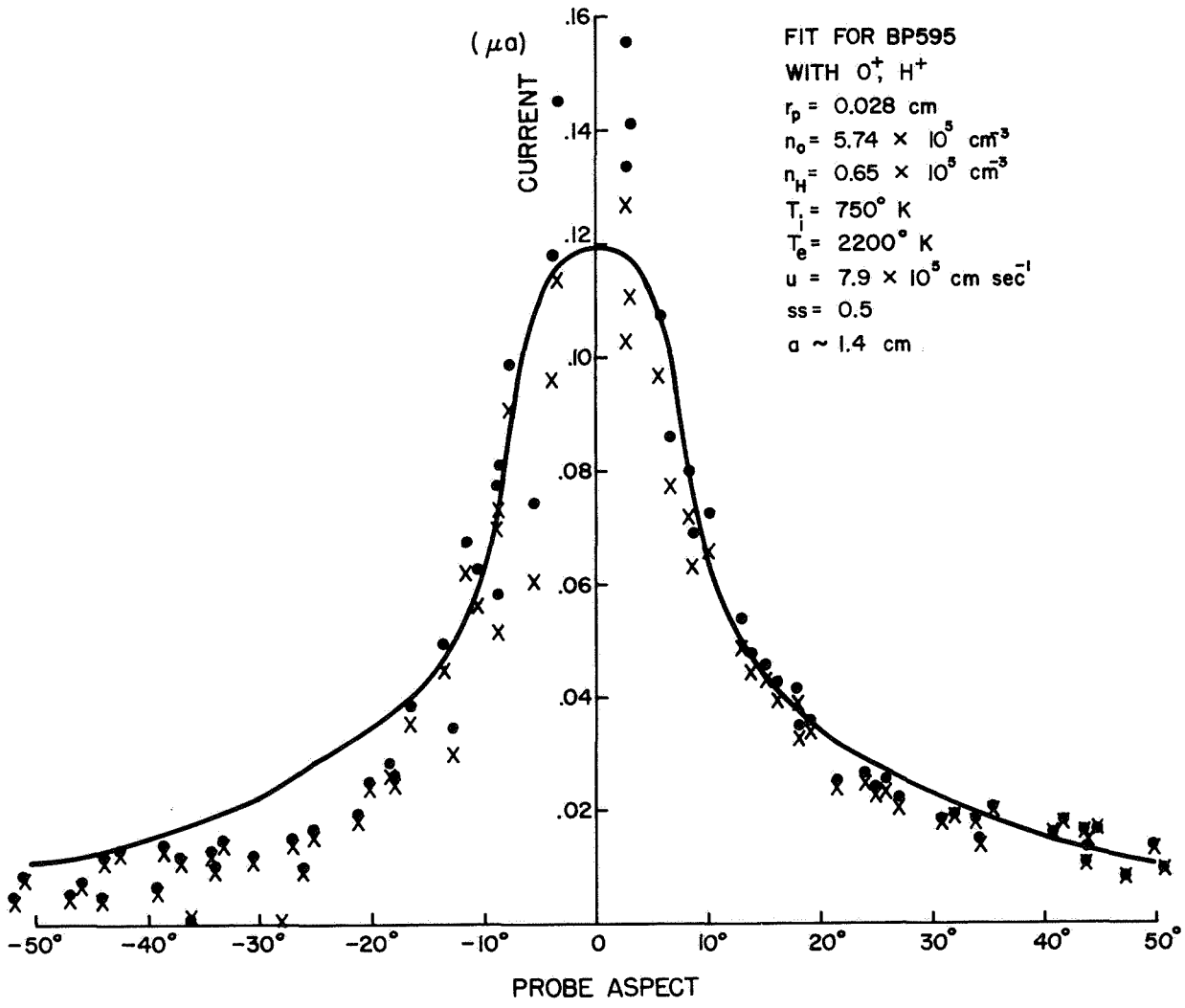
(μa)
CURRENT
.16
.14
.12
.10
.08
.06
.04
.02
FIT FOR BP595
WITH O^+, H^+
r_p = 0.028 cm
n_o = 5.74 × 10^5 cm^{-3}
n_H = 0.65 × 10^5 cm^{-3}
T_i = 750° K
T_e = 2200° K
u = 7.9 × 10^5 cm sec^{-1}
ss = 0.5
a ~ 1.4 cm
-50°
-40°
-30°
-20°
-10°
0
10°
20°
30°
40°
50°
PROBE ASPECT

FIG. 19

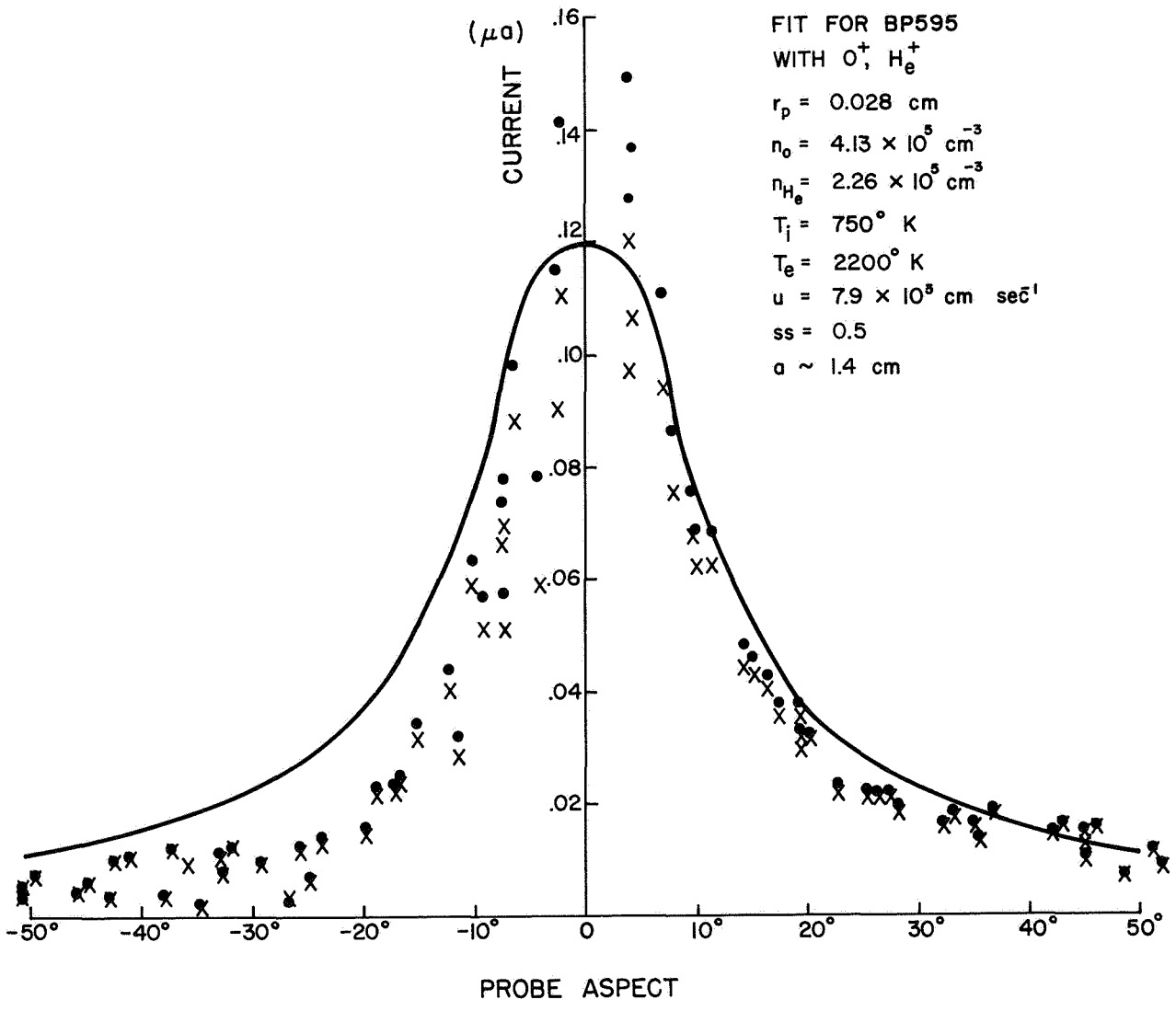
(μa)
CURRENT
.16
.14
.12
.10
.08
.06
.04
.02
FIT FOR BP595
WITH O^+, H_e^+
r_p = 0.028 cm
n_o = 4.13 × 10^5 cm^{-3}
n_{H_e} = 2.26 × 10^5 cm^{-3}
T_i = 750° K
T_e = 2200° K
u = 7.9 × 10^5 cm sec^{-1}
ss = 0.5
a ~ 1.4 cm
-50°
-40°
-30°
-20°
-10°
0
10°
20°
30°
40°
50°
PROBE ASPECT

FIG. 20

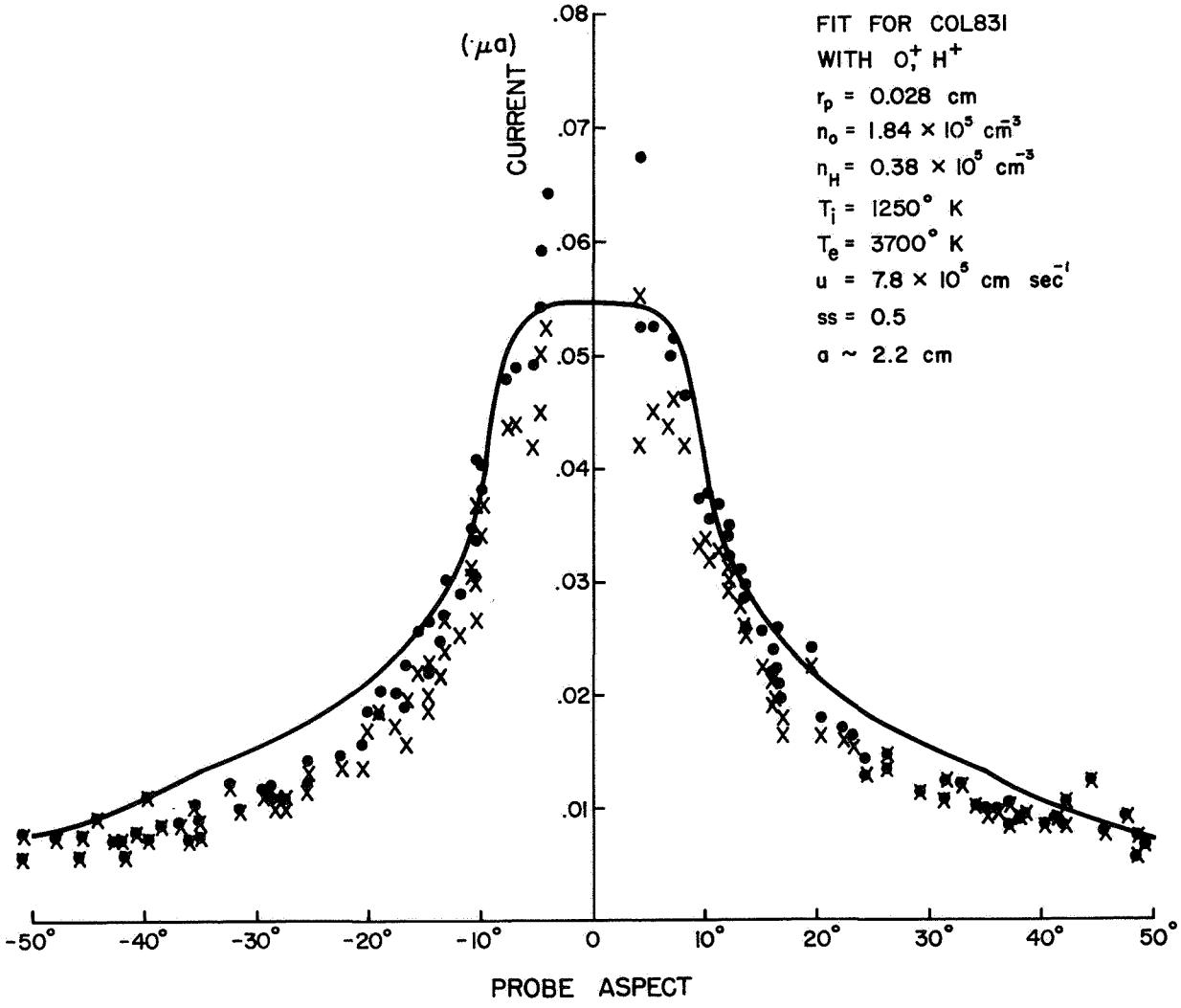
FIT FOR COL831
WITH O^+, H^+
r_p = 0.028 cm
n_o = 1.84 × 10^5 cm^{-3}
n_H = 0.38 × 10^5 cm^{-3}
T_i = 1250° K
T_e = 3700° K
u = 7.8 × 10^5 cm sec^{-1}
ss = 0.5
a ~ 2.2 cm
(·μa)
CURRENT
.08
.07
.06
.05
.04
.03
.02
.01
-50°
-40°
-30°
-20°
-10°
0
10°
20°
30°
40°
50°
PROBE ASPECT

FIG. 21

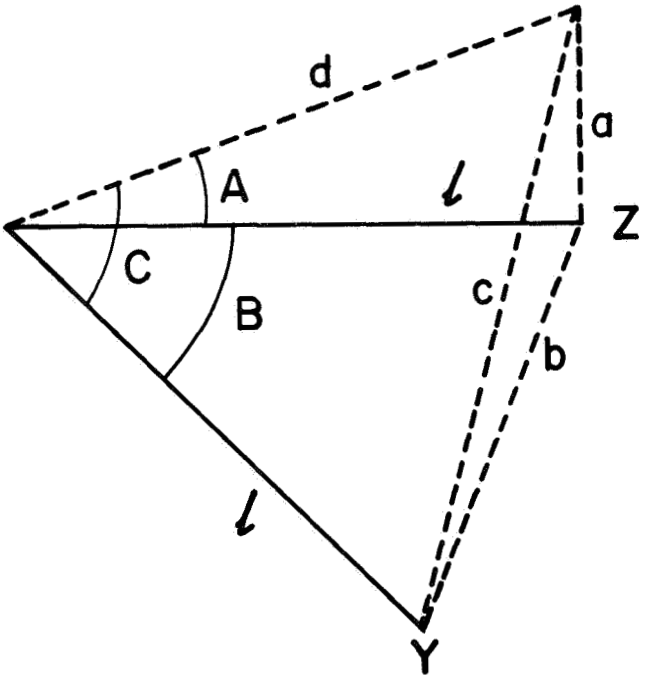

FIG. 22.

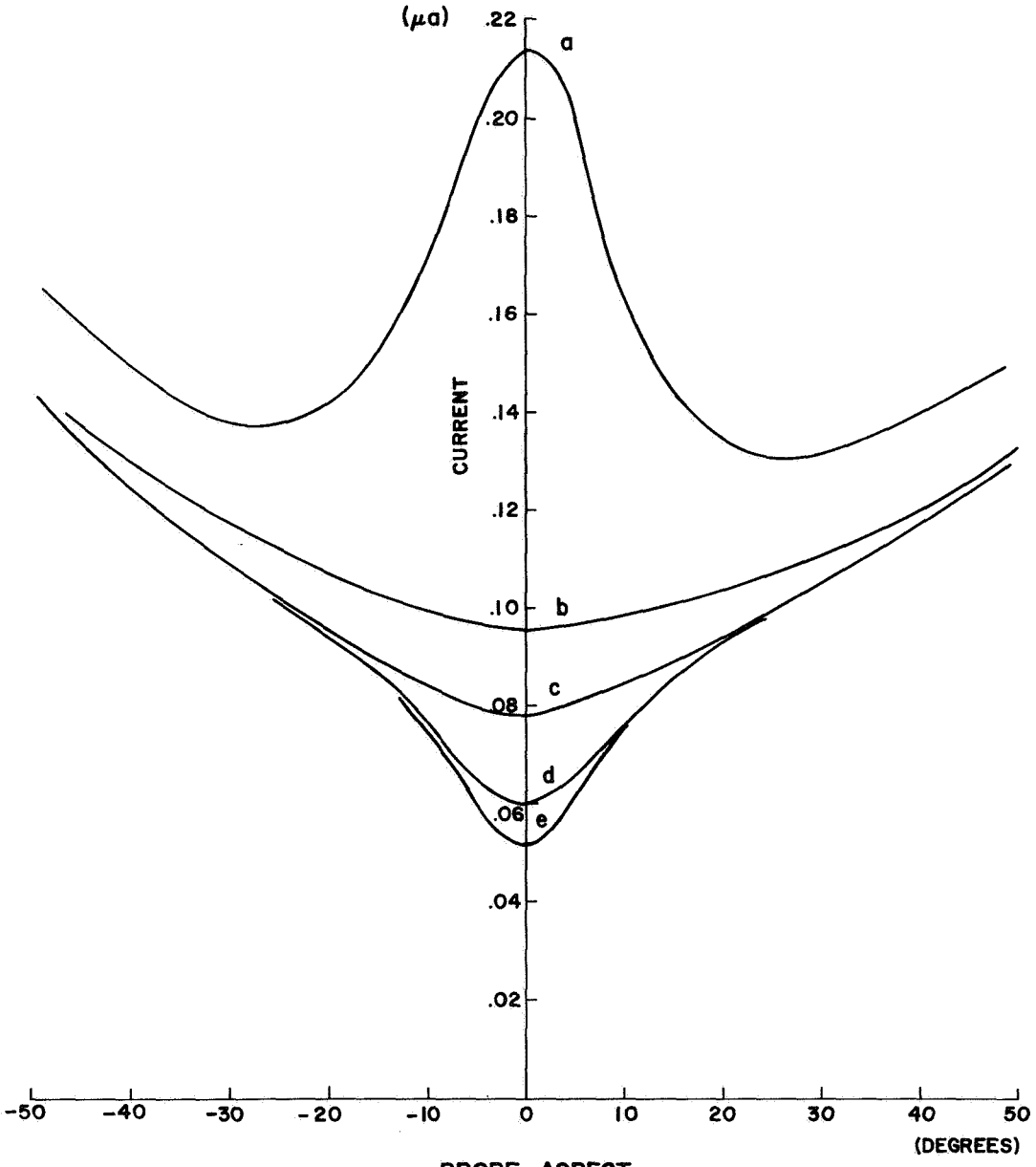
(μa)
.22
.20
.18
.16
.14
.12
.10
.08
.06
.04
.02
CURRENT
a
b
c
d
e
-50
-40
-30
-20
-10
0
10
20
30
40
50
(DEGREES)
PROBE ASPECT

FIG. 23